Accepted Manuscript

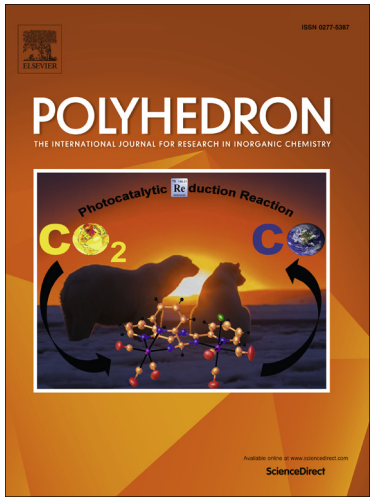

Synthesis and crystal structure of new monometallic and bimetallic copper(II) complexes with N-substituted isatin thiosemicarbazone ligands: Effects of the complexes on DNA/protein-binding property, DNA cleavage study and in *vitro* anticancer activity

Mathiyan Muralisankar, Surendran Sujith, Nattamai S.P. Bhuvanesh, Anandaram Sreekanth

PII: S0277-5387(16)30250-9
DOI: http://dx.doi.org/10.1016/j.poly.2016.06.017
Reference: POLY 12057

To appear in: *Polyhedron*

Received Date: 9 May 2016
Revised Date: 8 June 2016
Accepted Date: 9 June 2016

Please cite this article as: M. Muralisankar, S. Sujith, N. S.P. Bhuvanesh, A. Sreekanth, Synthesis and crystal structure of new monometallic and bimetallic copper(II) complexes with N-substituted isatin thiosemicarbazone ligands: Effects of the complexes on DNA/protein-binding property, DNA cleavage study and in *vitro* anticancer activity, *Polyhedron* (2016), doi: http://dx.doi.org/10.1016/j.poly.2016.06.017

This is a PDF file of an unedited manuscript that has been accepted for publication. As a service to our customers we are providing this early version of the manuscript. The manuscript will undergo copyediting, typesetting, and review of the resulting proof before it is published in its final form. Please note that during the production process errors may be discovered which could affect the content, and all legal disclaimers that apply to the journal pertain.

ACCEPTED MANUSCRIPT

Synthesis and crystal structure of new monometallic and bimetallic copper(II) complexes with N-substituted isatin thiosemicarbazone ligands: Effects of the complexes on DNA/protein-binding property, DNA cleavage study and in *vitro* anticancer activity

Mathiyan Muralisankar,[a] Surendran Sujith,[a] Nattamai S. P. Bhuvanesh[b] and Anandaram Sreekanth[a*]

[a] Department of Chemistry, National Institute of Technology, Tiruchirappalli - 620 015, India.

[b] Department of Chemistry, Texas A & M University, College Station, TX 77842, USA

ACCEPTED MANUSCRIPT

ACCEPTED MANUSCRIPT

Synthesis and crystal structure of new monometallic and bimetallic copper(II) complexes with N-substituted isatin thiosemicarbazone ligands: Effects of the complexes on DNA/protein-binding property, DNA cleavage study and in *vitro* anticancer activity

Mathiyan Muralisankar,[a] Surendran Sujith,[a] Nattamai S. P. Bhuvanesh[b] and Anandaram Sreekanth[a*]

Abstract

A novel series of N-substituted isatin thiosemicarbazone ligands (**L1–L3**) and their copper(II) complexes [Cu(II)(ITSC)] were synthesized and characterized by elemental analyses and UV Visible, FT-IR, ^{1}H & ^{13}C NMR / EPR and mass spectroscopic techniques. The molecular structures of **L1, L2, L3, 2** and **3** were confirmed by single crystal X-ray crystallography. The X-ray diffraction studies of the complexes **2** and **3** reveal the square planar and square pyramidal geometry. The binding affinity and binding mode of the monometallic and bimetallic complex toward calf thymus DNA (CT-DNA) and bovine serum albumin (BSA) were determined by UV-Vis and fluorescence spectrophotometric methods. Spectral evidences show intercalative mode of DNA binding with the copper(II) complexes. Complexes (**1, 2** and **3**) cleaved the pUC19 plasmid DNA in the absence of an external agent. An in vitro cytotoxicity study of the complex **3** found significant activity against human breast (MCF7) and lung (A549) cancer cell lines.

Keywords: monometallic and bimetallic copper(II) complexes; DNA/protein binding property; DNA cleavage; cytotoxicity.

*Corresponding Author E-mail address: sreekanth@nitt.edu; Tel: +91 431 2503642

ACCEPTED MANUSCRIPT

ACCEPTED MANUSCRIPT

1. INTRODUCTION

Metals have a vital role in biological systems and their role in cellular, subcellular functions are invariably recognized. The importance of metals is inevitable because they are the essential part of enzymes which involved in the metabolic or biochemical process. These elements required only in trace amount for cellular uptake and also it act as a catalyst [1]. The variable oxidation state of transition metal complexes made them as significant in bioinorganic chemistry and redox enzyme systems. The multiple reactive sites and the site specific substructures, stimulate the metal complexes as a promising candidate for artificial metallonucleases [2]. Nowadays the designing and study of new drugs which contain metals are one of the embryonic areas of research [3] In 1969 Barnett rosenbrg and co-workers discovered the antitumor activity of cis-platin and still now it is the widely used metal-based anticancer drugs against the cancers of ovaries, testicles etc. Even though it have some serious side effect like nephrotoxicity, cytotoxicity, vomiting, loss of hair etc [4]. The substantial side effect of cis-platin is mainly arise from its binding mode with DNA, were cisplatin form a covalent crosslink which inhibited the medicinal successes of cis-platin [5]. There for, the chemist has been paid much interest on design and synthesis of more biocompatible metal-based drugs, which are less toxic, high pharmacological effect, target-specific and non-covalent DNA binding mode. One of the most suitable alternatives is copper, because of its biocompatibility and versatility in coordination. The assumption that copper like endogenous metals may less toxic for normal cells with respect to cancer cells [8]. Investigation of literature shows that there are much copper contain complexes which show potential antitumor, anticancer activities [9-12]. The pharmacological effect of mononuclear copper complexes are extensively studied, but studies on binuclear copper complexes are very few till to date. There is a number of proteins which holding binuclear centers and they have a vital role in biological functioning [13-15] this fact stimulated us to synthesis and compare between mono nuclear and binuclear copper complexes of thiosemicarbazone ligands. Many metal-based anticancer drugs exert their pharmacological effect through binding to DNA or protein. So the study of the interaction between metal complexes with DNA or protein is momentous in the current scenario. The shape and the chemical structure of DNA provide a number of opportunities for interaction with metal complexes. The study interactions of drugs with proteins are very significant because human

ACCEPTED MANUSCRIPT

body have a number of proteins which all are assigned to different biological functions. Among the serum albumin proteins, the exploration of the interaction of copper complexes with bovine serum albumin (BSA) is very significant because of it is structurally homologous to human serum albumin (HSA). Examination of drug-protein interaction has also another impact that it influence the distribution, absorption, and metabolism of the drug [16-17].

We choose thiosemicarbazone derivatives as our ligands. The versatility in coordination and their capabilities such as intramolecular hydrogen bonding, bulkier coligand , and π-π stacking interactions inspire as to choose it [18,19]. An interesting attribute of the thiosemicarbazone is that in the solid state, they predominantly exist in the thione form, whereas in a solution state, they exhibit a thione- thiol tautomerism. The thiol form predominates in the solution state, and deprotonation at the thiolatc sulfur render the thioscmicarbazonc an anionic ligand, which can effectively coordinate to a metal atom. In addition, it should be noted that in the thiol form, there is an effective conjugation along the thiosemicarbazone skeleton thus giving rise to an efficient electron delocalization along the moiety. Also, literature shows that thiosemicarbazone based compounds show variety of medicinal properties such as anticancer, antitumour, antifungal, antibacterial, antiviral, antimalarial, antifilarial and anti-HIV activities [20-27]. Hence, we are amalgamate copper metal with thiosemicarbazone ligands and we compare the biological activity of mono and binuclear complexes. In the present work, we are synthesized and characterized the thiosemicarbazone based mono and bimetallic copper complexes. The interaction of complexes with DNA and protein were studied, also, the biological activity examined.

2. Experimental

2.1. Materials and methods

All the chemicals were purchased from Sigma Aldrich / Merck and used as received. Solvents were purified by distillation and retained under inert atmosphere. The melting points were determined on Lab India instrument and are uncorrected. The elemental analyses were performed using a Vario EL–III CHNS analyzer. Magnetic susceptibilities were measured using Sherwood scientific auto magnetic susceptibility balance. FT-IR spectra were recorded in the range of 400-4000 cm^{-1} (KBr pellets) and far-IR spectra were recorded in the range of 400-30 cm^{-1} (polyethylene pellets) using a PerkinElmer Frontier FT-IR/FIR spectrometer. UV-Visible

ACCEPTED MANUSCRIPT

spectra were recorded in the range of 900-250nm using a PG Instruments T90+UV-visible spectrophotometer in DMF solution. Emission spectra were measured on a Jasco V-630 spectrophotometer using 5% DMF in buffer as the solvent. NMR spectra were recorded in $CDCl_3$ by using TMS as an internal standard on a Bruker 400 MHz spectrometer. EPR spectra were recorded on a JEOL EPR spectrometer at liquid nitrogen temperature, operating at X-band frequency (9.1 GHz).

2.2. Synthesis of ligands (L1- L3).

Step 1: Ethanolic solution of cyclohexyl isothiocyanate (0.706 g, 0.005 mole) and hydrazine hydrate (0.250 g, 0.005 mole) were mixed with constant stirring. The stirring was continued for one more hour and the white product, N(4)-cyclohexylthiosemicarbazide formed was filtered, washed, dried and recrystallized from ethanol. Yield: 91%

Step 2: N(4)-cyclohexylthiosemicarbazide (0.173 g, 0.001 mole) was dissolved in methanol (20 mL) and was added to the appropriate ketone's [1-(prop-2-yn-1-yl)indoline-2,3-dione (0.185 g, 0.001 mole); 1-allylindoline-2,3-dione (0.187 g, 0.001 mole) and 1-benzylindoline-2,3-dione (0.237 g, 0.001 mole)] dissolved in methanol (20 mL), reflux continuously for 6 h after a few drops of acetic acid. The yellow product formed was filtered off, washed with cold ethanol and ether, and dried in vacuo. It was recrystallized from CH_3OH/C_2H_3N mixture (1:1) to get yellow colored crystals suitable for X-ray studies were obtained from slow evaporation of the reaction mixture for 10-15 days in all three cases.

2.2.1 N-cyclohexyl-2-(2-oxo-1-(prop-2-yn-1-yl)indolin-3-ylidene)hydrazinecarbothioamide (L1)

N(4)-cyclohexylthiosemicarbazide (0.173 g, 0.001 mole), 1-(prop-2-yn-1-yl)indoline-2,3-dione (0.185 g, 0.001 mole) were used. Yield: 82%. Yellow. 2 ^{o}C. Anal. Calc. $C_{18}H_{20}N_4OS$ (%): C, 63.50; H, 5.92; N, 16.46; S, 9.42. Found: C, 63.22; H, 5.68; N, 16.41; S, 9.41. UV–Vis (DMF): λ_{max}, nm (ε, $dm^3mol^{-1}cm^{-1}$) 268 (53600), 366 (73200). FT-IR (KBr): υ, cm^{-1} 3344 (N–H), 3223 (N–H), 1689 (C=O), 1526 (C=N), 1353 (C=S). ^{1}H NMR (400 MHz, $CDCl_3$): δ, ppm 12.56 (s, 1H), 7.66 – 7.59 (m, 2H), 7.40 (td, *J* = 7.8, 1.2 Hz, 1H), 7.14 (td, *J* = 7.6, 0.8 Hz, 1H), 7.09 (d, *J* = 7.9 Hz, 1H), 4.53 (d, *J* = 2.5 Hz, 2H), 4.36 – 4.25 (m, 1H), 2.26 (t, *J* = 2.5 Hz, 1H), 2.14 (dd, *J* = 12.0, 3.0 Hz, 2H), 1.80 – 1.72 (m, 2H), 1.71 – 1.62 (m, 1H), 1.52 – 1.41 (m, 2H), 1.32 (dd, *J* = 11.4, 8.4 Hz, 2H), 1.21 (ddd, *J* = 15.3, 8.1, 3.4 Hz, 1H). ^{13}C NMR (100 MHz, $CDCl_3$): δ, ppm 176.4 (C=S), 160.1 (C=O), 141.7 (C=N), 131.1, 130.0, 123.5, 120.6, 119.7,

ACCEPTED MANUSCRIPT

110.1 (aromatic C), 76.1, 73.0 (propa), 53.4, 28.9, 25.5, 24.8 (Cyclohexane C). ESI-MS m/z=341.14 $[M+1]^+$

2.2.2 2-(1-allyl-2-oxoindolin-3-ylidene)-N-cyclohexylhydrazinecarbothioamide (L2)

N(4)-cyclohexylthiosemicarbazide (0.173 g, 0.001 mole), 1-allylindoline-2,3-dione (0.187 g, 0.001 mole) were used. Yield: 80%. Yellow. m.p.: 180 ^oC. Anal. Calc. $C_{18}H_{22}N_4OS$ (%): C, 63.13; H, 6.48; N, 16.36; S, 9.36. Found: C, 63.10; H, 6.42; N, 16.32; S, 9.35. UV–Vis (DMF): λ_{max}, nm (ε, $dm^3mol^{-1}cm^{-1}$) 265 (53000), 367 (79400). FT-IR (KBr): υ, cm^{-1} 3349 (N–H), 3258 (N–H), 1684 (C=O), 1521 (C=N), 1344 (C=S). ^1H NMR (500 MHz, $CDCl_3$): δ, ppm 12.57 (s, 1H), 7.65 (d, *J* = 7.3 Hz, 1H), 7.62 (d, *J* = 7.4 Hz, 1H), 7.41 (t, *J* = 7.6 Hz, 1H), 7.15 (t, *J* = 7.4 Hz, 1H), 7.10 (d, *J* = 7.8 Hz, 1H), 4.54 (s, 2H), 4.37 – 4.28 (m, 1H), 2.28 (t, *J* = 7.2 Hz, 1H), 2.15 (d, *J* = 10.3 Hz, 2H), 1.78 (d, *J* = 12.6 Hz, 3H), 1.67 (d, *J* = 12.4 Hz, 2H), 1.46 (dd, *J* = 24.1, 12.1 Hz, 3H), 1.35 (dt, *J* = 20.8, 10.6 Hz, 2H), 1.31 – 1.21 (m, 1H). ^{13}C NMR (100 MHz, $CDCl_3$): δ, ppm 176.5 (C=S), 160.7 (C=O), 142.8 (C=N), 131.0, 130.8, 123.1, 120.0, 119.6, 118.3 (aromatic C), 130.5, 109.9 ( ), 53.3, 32.5, 25.6, 24.8 (Cyclohexane C). ESI-MS m/z=343.15 $[M+1]^+$

2.2.3. 2-(1-benzyl-2-oxoindolin-3-ylidene)-N-cyclohexylhydrazinecarbothioamide (L3)

N(4)-cyclohexylthiosemicarbazide (0.173 g, 0.001 mole), 1-benzylindoline-2,3-dione (0.237 g, 0.001 mole) were used. Yield: 83%. Yellow. m.p.: 168 ^oC. Anal. Calc. $C_{22}H_{24}N_4OS$ (%): C, 67.32; H, 6.16; N, 14.27; S, 8.17. Found: C, 67.28; H, 6.08; N, 14.22; S, 8.15. UV–Vis (DMF): λ_{max}, nm (ε, $dm^3mol^{-1}cm^{-1}$) 281 (56200), 369 (73800). FT-IR (KBr): υ, cm^{-1} 3343 (N–H), 3229 (N–H), 1687 (C=O), 1523 (C=N), 1348 (C=S). ^1H NMR (500 MHz, $CDCl_3$): δ, ppm 12.75 (s, 1H), 7.67 (d, *J* = 7.9 Hz, 1H), 7.60 (d, *J* = 7.5 Hz, 1H), 7.35 – 7.24 (m, 6H), 7.08 (t, *J* = 7.6 Hz, 1H), 6.79 (d, *J* = 7.9 Hz, 1H), 4.94 (s, 2H), 4.39 – 4.29 (m, 1H), 2.16 (d, *J* = 10.8 Hz, 1H), 1.78 (d, *J* = 13.2 Hz, 2H), 1.72 – 1.63 (m, 2H), 1.47 (dd, *J* = 24.5, 12.1 Hz, 2H), 1.36 (dd, *J* = 22.2, 10.8 Hz, 2H), 1.26 (dd, *J* = 24.2, 12.0 Hz, 1H). ^{13}C NMR (100 MHz, $CDCl_3$): δ, ppm 176.5 (C=S), 161.1 (C=O), 142.8 (C=N), 135.1, 131.0, 130.5, 129.0, 128.1, 127.5, 123.2, 120.6, 119.7, 110.1 (aromatic C), 53.3, 32.5, 25.6, 24.8 (Cyclohexane C). ESI-MS m/z=393.17 $[M+1]^+$

2.3 Synthesis of copper (II) complexes (1, 2 and 3)

Step 3: The chloroformic solution of $CuCl_2.2H_2O$ (0.001 mole) was added into the solution of an appropriate substituted isatin thiosemicarbazone ligands (0.001 mole) in methanol. The reaction mixture was stirred for 2 hours at room temputure, and then the precipitate formed

ACCEPTED MANUSCRIPT

was filtered and washed with chloroform. The suitable crystals for X-ray diffraction were grown from CH_3OH/C_2H_3N mixture (1:1) to get blackish brown colored crystals suitable for X-ray studies were obtained from slow evaporation of the reaction mixture for 20 days in complexes **2** and **3**.

2.3.1 2-(2-oxo-1-(prop-2-yn-1-yl)indolin-3-ylidene)-N-cyclohexyl-hydrazinecarbothioamide copper(II) (1)

$CuCl_2.2H_2O$ (0.170 g, 0.001 mole), L1 (0.340 g, 0.001 mole) were used. Yield: 75%. Light brown block solid. m.p.: 239 °C. Anal. Calcd. For $C_{18}H_{19}ClCuN_4OS$: C, 49.31; H, 4.37; N, 12.78; S, 7.31. Found: C, 49.36; H, 4.35; N, 12.76; S, 8.56. UV–Vis (DMF): λ_{max}, nm (ε, $dm^3mol^{-1}cm^{-1}$) 266 (51466), 359 (15400), 433 (18933). FT-IR (KBr): υ, cm^{-1} 3245 (N–H), 1640 (C=O), 1503 (C=N), 1245 (C= S) and far-IR (Polyethylene) υ, cm^{-1} 362 (Cu–N_{azo}), 348 (Cu-S), 316 (Cu-Cl). Epr (LNT): 'g' values 2.25, 2.04

2.3.2 2-(1-allyl-2-oxoindolin-3-ylidene)-N-cyclohexylhydrazinecarbothioamide copper(II) (2)

$CuCl_2.2H_2O$ (0.170 g, 0.001 mole), L2 (0.342 g, 0.001 mole) were used. Yield: 79%. Light brown block solid. m.p.: 243 °C. Anal. Calcd. For $C_{18}H_{21}ClCuN_4OS$: C, 49.08; H, 4.81; N, 12.72; S, 7.28. Found: C, 49.61; H, 4.82; N, 12.68; S, 7.22. UV–Vis (DMF): λ_{max}, nm (ε, $dm^3mol^{-1}cm^{-1}$) 265 (50666), 356 (26000), 424 (32066). FT-IR (KBr): υ, cm^{-1} 3257 (N–H), 1634 (C=O), 1508 (C=N), 1263 (C= S) and far-IR (Polyethylene) υ, cm^{-1} 369 (Cu–N_{azo}), 328 (Cu-S), 302 (Cu-Cl). Epr (LNT): 'g' values 2.22, 2.05

2.3.3 2-(1-benzyl-2-oxoindolin-3-ylidene)-N-cyclohexylhydrazinecarbothioamide copper(II) (3)

$CuCl_2.2H_2O$ (0.170 g, 0.001 mole), L3 (0.392 g, 0.001 mole) were used. Yield: 61%. Light brown block solid. m.p.: 252 °C. Anal. Calcd. For $C_{44}H_{46}Cl_2Cu_2N_8O_2S_2$: C, 53.87; H, 4.73; N, 11.42; S, 6.54. Found: C, 53.91; H, 4.74; N, 11.38; S, 6.51. UV–Vis (DMF): λ_{max}, nm (ε, $dm^3mol^{-1}cm^{-1}$) 265 (46533), 373 (25800), 423 (21733). FT-IR (KBr): υ, cm^{-1} 3221 (N–H), 1634 (C=O), 1508 (C=N), 1274 (C= S) and far-IR (Polyethylene) υ, cm^{-1} 371 (Cu–N_{azo}), 348 (Cu-S), 316 (Cu-Cl). Epr (LNT): 'g' values 2.04, 2.00

2.4. Single crystal X-ray diffraction studies

ACCEPTED MANUSCRIPT

A Bruker APEX2 or Bruker GADDS X-ray (three-circle) diffractometer was employed for crystal screening, unit cell determination, and data collection. The X-ray radiation employed was generated from a Mo sealed X-ray tube (K_α = 0.70173 Å; 40 kV, 40 mA) for **L1, L2, L3, 2** and **3** fitted with a graphite monochromator (175 mm collimator with 0.5 mm pinholes). Sixty data frames were taken at widths of 0.5°. These reflections were used in the auto-indexing procedure to determine the unit cell. A suitable cell was found and refined by nonlinear least squares and Bravais lattice procedures. The unit cell was verified by examination of the *h k l* overlays on several frames of data by comparing with both the orientation matrices. No super-cell or erroneous reflections were observed. After careful examination of the unit cell, a standard data collection procedure was initiated using omega scans. Integrated intensity information for each reflection was obtained by reduction of the data frames with the program APEX2 [28]. The integration method employed a three dimensional profiling algorithm and all data were corrected for Lorentz and polarization factors, as well as for crystal decay effects. Finally, the data were merged and scaled to produce a suitable data set. The absorption correction program SADABS [29] was employed to correct the data for absorption effects. Systematic reflection conditions and statistical tests of the data suggested the space group. Solution was obtained readily using XT/XS in APEX2 [30]. Hydrogen atoms were placed in idealized positions and were set riding on the respective parent atoms. All non-hydrogen atoms were refined with anisotropic thermal parameters. The structure was refined (weighted least squares refinement on F^2) to convergence [31]. Olex2 was employed for the final data presentation and structure plots [30].

2.5. DNA binding studies

The binding of metal complexes with CT DNA was carried out in Tris HCl/NaCl buffer (pH 7.2). The bulk solution of CT DNA was prepared by diluting the CT DNA using Tris HCl/NaCl buffer followed by stirring at 4 °C for three days, and kept at 4 °C for not more than a week. The stock solution of CT DNA gave a ratio of UV absorbance at 260 and 280 nm (A260/A280) of 1.9, indicating that the DNA was sufficiently free of proteins. The bulk DNA solution was further diluted to 10 folds to show maximum absorbance at 260 nm. The absorption coefficient of CT DNA was 6600 cm^{-1} M^{-1} per nucleotide [32]. Cu(II) complexes of required concentration were prepared by dissolving the calculated amount of the complexes in 5% DMF/Tris HCl/NaCl. Complex solution of concentration 15 µM was taken in cuvette and CT

ACCEPTED MANUSCRIPT

DNA of equivalent concentration (0–50 μM) was added each time and the significant absorbance change was noted.

The competitive binding of each complex with EB has been investigated by fluorescence spectroscopic technique in order to examine whether the complex can displace EB from its CT DNA-EB complex. Ethidium bromide solution was prepared using Tris HCl/NaCl buffer (pH 7.2). The test solution was added in aliquots of 2.5 μM concentration to DNA-EB and the change in fluorescence intensities at 607 nm (520 nm excitation) was noted down.

Viscosity experiments were carried out using a semi micro viscometer maintained at 27 °C in a thermostatic water bath. DNA samples (0.5 μM) were prepared by sonication in order to minimize complexities arising from DNA flexibility. Flow time was measured three times for each sample and an average flow time was calculated. The values of relative specific viscosity (η/η^0), where η is the relative viscosity of DNA in the presence of the complex and η0 I s the relative viscosity of DNA alone, were plotted against 1/R (1/R = [compound]/[DNA]). Relative viscosity (η^0) values were calculated from the observed flow time of the DNA solution (t) corrected for the flow time of the buffer alone (t^0), using the expression $\eta^0 = (t - t^0)/t^0$ [33].

2.6. Protein binding studies

The binding of Cu(II) complexes (**1**, **2** and **3**) with BSA was studied using fluorescence spectra recorded at a fixed excitation wavelength corresponding to BSA at 280 nm and monitoring the emission at 335 nm. The excitation and emission slit widths and scan rates were constantly maintained for all the experiments. Stock solution of BSA was prepared in 50 mM phosphate buffer (pH = 7.2) and stored in the dark at 4 °C for further use. Concentrated stock solutions of each test compound were prepared by dissolving them in DMF–phosphate buffer (5:95) and diluted with phosphate buffer to get required concentrations. 2.5 ml of BSA solution was titrated by successive additions of a 10^{-6} M stock solution of the complexes using a micropipette. For synchronous fluorescence spectra measurements, the same concentration of BSA and the complexes were used and the spectra were measured at two different Δλ (difference between the excitation and emission wavelengths of BSA) values of 15 and 60 nm.

2.7. DNA cleavage studies

A mixture of Tris buffer (5mMTris–HCl/50mMNaCl buffer, pH7.2), pUC19 plasmid DNA (150 μg mL^{-1}) and different amounts of the complexes (1–3) were incubated for 3 h at 37 ^oC. A dye solution (0.05% bromophenol blue and 5% glycerol) was added to the mixture prior to

ACCEPTED MANUSCRIPT

electrophoresis. The samples were then analyzed by 1.5% agarose gel electrophoresis [Tris–HCl/boric acid/EDTA (TBE) buffer, pH 8.0] for 2 h at 60 mV. The gel was stained with 0.5 μg mL^{-1} ethidium bromide, visualized by UV light and photographed. The extent of cleavage of pUC19 was determined by measuring the intensity of the bands using AlphaImager HP instrument.

2.8. Cytotoxic activity

Cytotoxicity of complexes (**1, 2** and **3**) was evaluated by using the MTT [3- (4,5 dimethyl thiazole-2-yl)-2,5-diphenyltetrazolium] assay [34]. The non-small lung adenocarcinoma cells (A549 cells) and human breast cancer cells (MCF-7) were plated separately in 96 well plates at a concentration of 1×10^5 cells/well. Complexes (**1**-**3**) of concentration ranging from 10-250 μM dissolved in DMSO were seeded to the wells. DMSO was used as the control. After 24 h, the wells were treated with 20 μL MTT [5 mg/ml phosphate buffered saline (PBS)] and incubated at 37 °C for 4 h. This colorimetric test is based on the selective ability of viable cells to reduce the tetrazolium component of MTT into purple coloured formazan crystals formed were dissolved in 200 μL DMSO. The absorbance of the solution was measured at a wavelength of 570 nm using a Beckmann Coulter Elisa plate. Triplicate samples were analyzed for each experiment. The percentage inhibition was calculated using the formula.

$$\frac{\textbf{Mean OD of the untreated cells (control)} - \textbf{Mean OD of the treated cells}}{\textbf{Mean OD of the untreated cells (control)}} \times \mathbf{10}$$

3. Results and discussion

3.1. Synthesis

Cyclohexylhydrazinecarbothioamide were synthesized using the standard procedure [35] (Scheme 1). The substituted heterocyclic based ligands (**L1**–**L3**) were synthesized by a condensation reaction from substituted heterocyclic based ketone and N(4) cyclohexylthio semicarbazide (Scheme **2**). The Cu(II) complexes were synthesized using $CuCl_2.2H_2O$ as the precursor (Scheme **3**). All the ligands and their Cu(II) complexes were characterized by elemental analyses and/or various spectroscopic techniques. The molecular structures of **L1, L2, L3, 2** and **3** were confirmed by single crystal X-ray diffraction studies.

ACCEPTED MANUSCRIPT

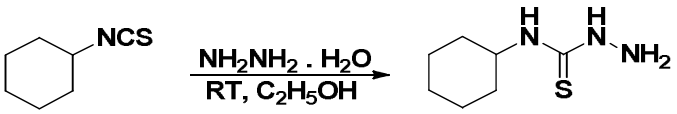

Scheme 1 Synthesis of N(4)-cyclohexylthiosemicarbazide.

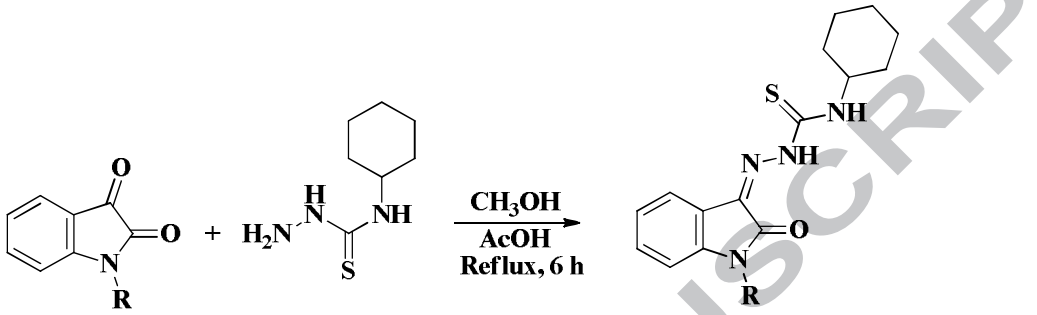

R = C_3H_3 (L1), C_3H_5 (L2) or C_7H_7 (L3)

Scheme 2 Synthesis of heterocyclic based thiosemicarbazone.

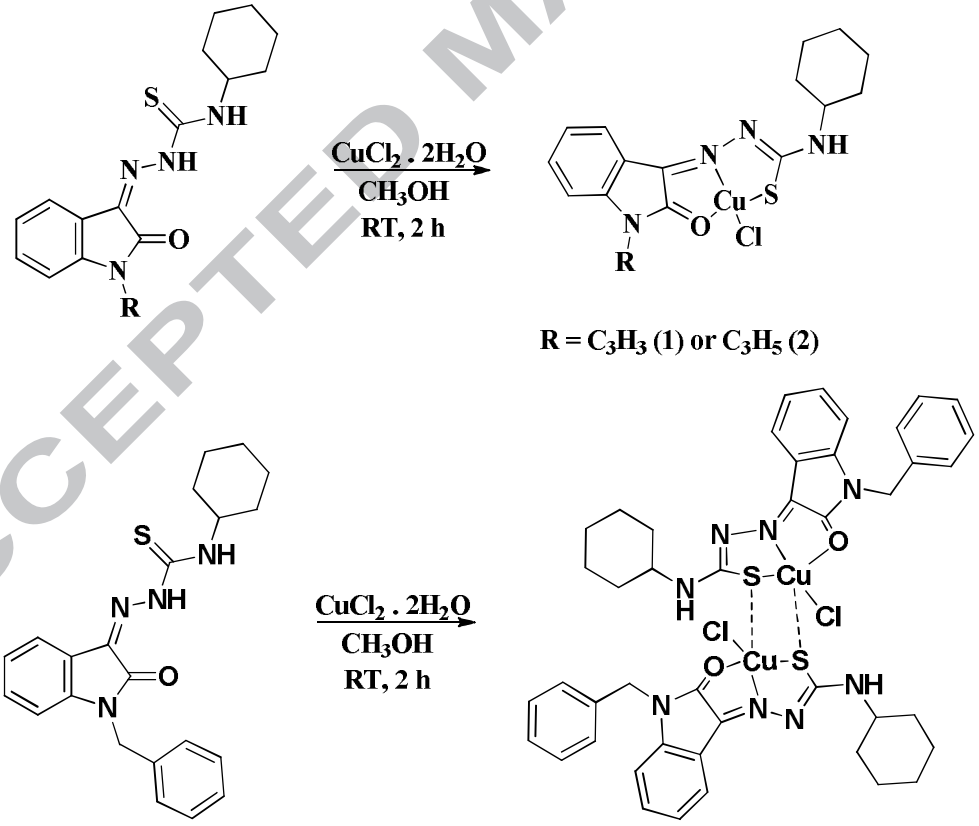

R = C_3H_3 (1) or C_3H_5 (2)

Scheme 3 Synthesis of copper(II) complexes.

ACCEPTED MANUSCRIPT

3.2. Spectroscopy

Electronic spectra of the ligands (**L1**, **L2** and **L3**) showed two strong absorption bands around 265-281 and 366-369 nm, which were assigned to $\pi \rightarrow \pi^*$ and $n \rightarrow \pi^*$ transitions respectively. The spectra of the complexes (**1**, **2** and **3**) exhibited three bands. The high intensity bands in the regions 264-266 nm correspond to intra ligand transitions. A less intense band at 358-373 nm has been assigned to ligand to metal charge transfer (LMCT) transitions respectively. The charge transfer transitions are observed in the region 421-432 nm. All complexes, taken in DMF at same concentration i.e. for fresh solution day one and after three days. There was no distinct changes observed in the UV-visible bands which clearly shows that the copper(II) complexes are stable in test solution. However, the Cu(ll) complexes appear to exist in a wide range of stereochemistry making it difficult to use electronic spectroscopy alone as a definitive tool for identifying the geometry. Similar assignments have been made for other copper(II) square planar and square pyramidal complexes [36,37].

In the FT-IR spectra of the solid state ligands (**L1, L2** and **L3**), two bands were observed for the stretching of N-H groups in the range of 3343-3349 and 3223-3258 cm^{-1}, which was absent in the complexes indicating deprotonation of the N-H group. The cyclohexene attached N-H groups appeared in the region 1321-1357 cm^{-1}. A strong band observed in the region 1684-1689 cm^{-1} in the FT-IR spectra of ligands was assigned to the C=O stretching vibration. This band was shifted to the lower frequency range of 1634-1640 cm^{-1} in the spectra of the complexes (**1**, **2** and **3**), consistent with the coordination of O to the metal ion. The characteristic band for C=S appeared in the region 1344-1353 cm^{-1} in the spectra of **L1**, **L2** and **L3** were shifted to lower frequency 1245-1274 cm^{-1} on complexation, indicating involvement of **S** coordination. The C=N stretching frequency of the ligands was observed at 1521-1526 cm^{-1}. During complexation there is a decrease in azomethine stretching frequency 1503-1514 cm^{-1}, which suggested that **N** coordinate to a metal ion. The Cu-N stretching frequencies for azomethine nitrogen are observed around 362-371 cm^{-1}. The presence of a new band in the 328-348 cm^{-1} range, which is assignable to Cu-S is another indication of the involvement of sulphur coordination. Bands at 302-316 cm^{-1} for the complexes are due to Cu-Cl stretching suggestive for terminally bonded chlorine [38].

ACCEPTED MANUSCRIPT

A sharp singlet observed at around 12.56–12.75 ppm in the ^{1}H NMR spectrum of the ligand **L1**-**L3** is assigned to H–N–C=S. The signals of cyclohexane protons in the all ligands appeared around 2.28–1.26 ppm. The signals around 7.67–6.79 ppm corresponding to aromatic protons of the ligands (**L1**–**L3**). In the ligand **L1** and **L2** the CH_2–C≡CH and CH_2–CH_2=CH_2 protons shows signal around 4.53, 4.36–4.25 and 4.54, 4.37–428 ppm respectively. The signal at 4.94 ppm corresponding to benzyl CH_2 protons of the ligand **L3**. ^{13}C NMR spectra of the ligands showed resonances due to thiocarbonyl (C=S), carbonyl carbon (C=O) and imine carbon (C=N) in the regions 176.4–176.5, 160.1–161.1 and 141.7–142.8 ppm respectively. The ligands **L1** (CH_2-C≡CH) and **L2** (CH_2–CH_2=CH_2), shows the carbon signals at 53.4, 76.1, 73.0 and 53.3, 130.5, 109.2 ppm respectively. The signal regions 53.3 ppm corresponding to benzyl carbon of **L3**. The cyclohexane carbons appeared around 42.0–43.5, 28.9–32.5, 25.5–25.6 and 24.8 ppm respectively. Chemical shift of all other aromatic and aliphatic protons/carbons was observed in the expected region [39].

The oxidation state of the central copper atom in the complexes was confirmed by the measurements of EPR spectroscopy. X-band CW EPR spectra of the Cu(II) complexes were recorded at LNT. For complexes **1**, **2** and **3** are EPR active due to the presence of an unpaired electron ($s = 1/2$) and the spin angular momentum quantum number can have values ($m_s = \pm 1/2$), which in the absence of external magnetic field the spin state of electrons are degenerate state. In the presence of magnetic field degeneracy no more present. The low energy sate has the spin magnetic moment aligned with the field and correspond to the quantum number ($m_s = -1/2$), while the high energy state ($m_s = +1/2$) has its moment opposed to the filed. Each spin state further spilt into four levels due to hyperfine splitting with nuclear spin of Cu(II) (I = 3/2) [40,41]. The transition between this split levels take place according to ($\Delta m_I = 0$). All the complexes (**1**, **2** and **3**) showed well resolved quartet hyperfine splitting typical of square planar and square pyramidal Cu(II) system (Fig. 1 and S1), which was confirmed by single crystal XRD technique. For all the complexes $g_{\|} > g\perp$ suggesting that the system is axial. The trend in the g value ($g_{\|} > g\perp > 2.00$) and the value of exchange interaction term (G > 4.0) suggested that the unpaired electron of Cu(II) ion is present in the dx^2–y^2 orbital (Table 1).

3.3. Single crystal X-ray crystallographic studies

ACCEPTED MANUSCRIPT

The molecular structure of ligands (**L1, L2** and **L3**) and the complexes (**2** and **3**) with the atomic labelling schemes are shown in the Fig. 2–6. Crystal data and some selected inter-atomic bond lengths and angles are given in the Tables 2–5. Ligands (**L1, L2** and **L3**) exists in the thione form as confirmed by the C=S bond length of 1.6723(16), 1.6696(18) and 1.6723 (14) Å. The crystal structures of the ligands showed the existence of an intra-molecular hydrogen bond between N–H and the carbonyl oxygen. An intra-molecular hydrogen bond between the N(3)–H(3) proton and O1 is present in ligands (**L1, L2** and **L3**) [2.769, 2.7850 and 2.7441 Å], creating a six-membered ring and favouring the Z-isomer with respect to the imine C=N bond. This hydrogen bond renders the isatin and TSc (N2–N3–C12/16–S1–N4) moieties essentially coplanar.

The complex **2** crystallized in monoclinic *P – 1* space group with one molecules of the ligand per copper. The copper (II) adopts a square planar geometry with binding of the ligands as monobasic tridentate (ONS) donors. The S1−C12 bond length (1.731 Å) in **2** is higher than that of **L2** [42]. There is an increase in the C–O and C–N bond lengths (involved in coordination) in **2** compared to **L2**. The Cu−S bond is longer than the Cu–Cl, Cu–O and Cu–N bonds [Cu(1)−S(1) 2.236 Å, Cu(1)−Cl(1) 2.192 Å, Cu(1)−O(1) 2.072 Å and Cu(1)−N(1) 1.970 Å], which are in the expected range for thiosemicarbazone complexes. The torsional angles in **2** are -2.4 [Cu(1) –S(1) –C(12) –N(2)], 176.7 [Cu(1) –S(1) –C(12) –N(4)], 179.0 [Cu(1)–O(1) –C(2) –N(3)].

The complex **3** crystallizes in monoclinic lattice with *P 1 21/n* 1 *space* group symmetry. Coordination extends the thiosemicarbazone moiety's S(1)−C(13) bond length from 1.684(3) Å (**L3**) to 2.2821(5) Å (**3**). The asymmetric unit is formed by one half of the molecule and the other half is related by a center of inversion in the Cu(1)−S(1)−Cu(1) −S(1)#1 ring. The coordination geometry at each Cu(II) is square pyramidal. The ligand **3** coordinates to the metal in a tridentate manner through its carbonyl oxygen, azomethine nitrogen and thiolate sulfur, after enolization and deprotonation, to form the basal plane along with one chlorine atom. The sulfur atom takes the axial position of the adjacent monomer like its counterpart does to form two distorted square pyramids. The Cu−Cu separation is found to be 3.541 Å. The τ value of 0.137 at metal centres indicates slight distortion from perfect square pyramidal geometry [43]. Thus, the two metal centres are bridged *via* sulfur atoms resulting in the formation of four five membered rings in which one copper atom is shared by two fused rings. A four membered ring involving

ACCEPTED MANUSCRIPT

the copper atoms and the sulfur atoms is also formed. The five membered ring Cu(1), O(1), C(2), C(1), is approximately planar with a maximum deviation of −3.6(2) Å for C(2), but Cu(1), S(1), C(16), N(2) ring is slightly distorted as evidenced by the maximum deviation of −4.31(16) Å; likewise for their counterpart rings. The four membered ring Cu(1)−S(1)−Cu(1)#1 makes an angle of 88.283(17) Å with the mean plane of bicyclic chelate system O(1), C(2), C(1), N(1), N(2), C(16), S(l), Cu(1) which is slightly distorted from planarity. The present compound contains the shortest apical Cu–S distance reported to date for square-pyramidal Cu(II) complexes of N^4–substituted isatin thiosemicarbazones [44]. The free ligand (**L3**) exists as the thione tautomer and coordinates to the Cu(II) atom in the deprotonated thiolate form, thus rendering a single-bond character for the C−S bond. Similarly, coordination of the azomethine N atom and carbonyl O atom to the central Cu(II) atom results in a redistribution of the electron density along the thiosemicarbazone chain, giving rise to changes in the bond distances along the moiety compared with those of the uncoordinated thiosemicarbazone. There is increase in the C=N and C=O bond distance (involved in coordination) in complex **3** compared to ligand **L3**. The Cu−S bond is longer than the Cu–Cl, Cu–O and Cu–N bonds [Cu(1)−S(1) 2.2821(13) Å, Cu(1)−Cl 2.2140(5) Å, Cu(1)−O(1) 2.1069(13) Å and Cu(1)−N(1) 1.9812(16) Å.

3.4. DNA binding studies

For evaluating the potentials of antitumor activities of any new complexes, DNA binding is the significant footstep for chemical nuclease activity of the metal complexes. The understanding of the interaction between DNA and a complexes to be investigated is of most importance. Hence the mode and tendency for the binding of complexes to CT DNA were studied with different methods.

3.4.1. Electronic absorption titration

Electronic absorption spectroscopic studies are one of most reliable techniques have been used to investigate the interactions of metal complexes with DNA. When metal complexes are bound to a DNA, there should be different types of binding modes occur, non-covalent binding, metal coordination to the nucleobases, intercalation, phosphate backbone binding. From the change in absorbance and shift in wavelengths, we can understand the binding nature of metal complexes with DNA. In general, the intercalative mode of binding due to the strong stacking interaction between an aromatic chromophore and the base pairs of DNA, usually results in hypochromism along with or without a small red or blue shift [45]. The extent of shift and hypochromism

ACCEPTED MANUSCRIPT

correlate with the intercalative binding strength. The absorption spectrum of the complexes **1, 2** and **3** in the absence and presence of CT DNA are shown in Fig. 7 and S2. Upon increasing concentration of DNA, the absorption band of the complexes **1, 2** and **3** exhibited a hypochromism (Δε, 23, 28 and 38%) with a red shift of (1, 2 and 5) nm respectively. These results suggested that all the new copper complexes bind to the DNA helix via intercalation, due to stacking interaction between the planar aromatic chromophore and the base pairs of DNA. Monometallic complexes of **1** and **2** showed less hypochromicity than the bimetallic complex **3**, indicating that the binding strength of bimetallic complexes is much stronger than the other complexes. The binding constant of the complexes with CT DNA (K_b) was obtained from the ratio of slope to intercept in plots [DNA]/($\varepsilon_a - \varepsilon_f$) *versus* [DNA] according to the equation [46] [DNA]/($\varepsilon_a - \varepsilon_f$) = [DNA]/($\varepsilon_b - \varepsilon_f$) + 1/$K_b$ ($\varepsilon_b - \varepsilon_f$) where [DNA] is the concentration of DNA in base pairs, ε_a is the apparent extinction coefficient value found by calculating A(observed)/[complex], ε_f is the extinction coefficient for the free compound, and ε_b is the extinction coefficient for the compound in the fully bound form. Each set of data, when fitted into the above equation, gave a straight line with a slope of 1/($\varepsilon_b - \varepsilon_f$) and an y-intercept of 1/K_b($\varepsilon_b - \varepsilon_f$) and the value of K_b was determined from the ratio of slope to intercept (Fig. 8). The magnitudes of intrinsic binding constants (K_b) are shown in Table 6. The observed values of K_b revealed that the Cu(II) complexes bind to DNA *via* intercalative mode [47]. The K_b values were found to be in the range of $1.49 - 1.72 \times 10^5$ M^{-1}. Complex **3** showed better DNA binding affinity compared to the other complexes. Which is due to the geometry of the bimetallic copper complex bridged with sulphur plays profound effect on DNA binding abilities, which cause the considerable difference in the K_b value of bimetallic copper complex **3** over than mono metallic copper complexes **1** and **2**.

3.4.2. Viscosity measurements

The nature of binding of the metal complexes to the CT DNA was further investigate by viscosity measurements. For intercalation bond between a copper(II) complexes and the base pairs of DNA forces these base pairs away from each other and therefore, unwinding the double helix and lengthening a given amount of DNA which in turn, increases the viscosity of the DNA solution Fig .12. The increase in the viscosity of DNA follows the order **3> 2 > 1**, but lower than that for the standard DNA intercalator EB. Thus, all these observations suggest that the N-

ACCEPTED MANUSCRIPT

substituted aromatic ring of complex **3** showed enhanced binding ability compared to other complexes.

3.4.3. Ethidium bromide displacement study

The absorption titration results indicate that the new copper(II) complexes effectively bind to DNA, In order to get further evidences for binding mode and to compare their binding affinities, ethidium bromide displacement experiments were carried out. Usually, intense fluorescent light is emitted from EB in the presence of CT DNA due to the strong intercalation between adjacent DNA base pairs in the double helix; EB is considered to be a typical indicator of intercalation [48]. Hence, EB displacement technique can be used to obtain indirect evidence for the DNA binding mode. The displacement technique is based on the decrease of fluorescence intensity due to the displacement of EB from a DNA sequence by a quencher and the quenching is due to the reduction of the number of binding sites on the DNA that is available to the EB. The changes observed in the fluorescence quenching spectra of DNA-bound EB in the presence of copper(II) complexes (0-50 μM) are shown in Fig. 10 and S3 which illustrate that as copper(II) complexes intercalate into DNA, it leads to a decrease in the binding sites of DNA available for EB, resulting in a decrease in the fluorescence intensity of the CT DNA-EB system. Fluorescence quenching is explained by the Stern-Volmer equation [49] $F^o/F = 1 + K_q$ [Q] where F^o and F are the fluorescence intensities in the absence and presence of complex respectively, K_q is a linear Stern-Volmer quenching constant, and [Q] is the concentration of complex. The slope of the plot of F^o/F *versus* [Q] gave K_q (Fig. 9). The apparent DNA binding constant (K_{app}) values was calculated by using the equation K_{EB} [EB] = K_{app} [complex] where [complex] is the complex concentration at 50% reduction in the fluorescence intensity of EB, $K_{EB} = 1.0 \times 10^7$ M^{-1} and [EB] = 5 μM. The quenching constant K_q and K_{app} values follows order **3> 2> 1,** which follows the same order as discussed in the absorption titration and values are listed in Table 6.

3.4.4 Electrochemical titration

The cyclic voltammetric technique can be used to investigate the interaction between the metal complexes and DNA, which also provides an important complement to the previously used spectral experiments [50]. The understanding of the interaction between DNA and a complexes, the cyclic voltammetric technique was carried out and the results are given in Fig. 11 and S4. Obviously, in the absence of CT DNA, both of the monometallic and bimetallic complexes (**1, 2** and **3**) have a couple of waves corresponding to Cu(II)/Cu(I) with the cathodic (E_{Pc}) and anodic

ACCEPTED MANUSCRIPT

peak potential (E_{Pa}) being −1.03 and V −0.75 for the complex **1**, −1.04 V and −0.77 V for the complex **2** and -1.06 V and −0.76 for the complex **3**, respectively. The separations of anodic and cathodic peaks (ΔE_p) are found to be 0.28 V (**1**), 0.27 V (**2**) and 0.30 V (**3**). The formal potentials of the Cu(I)/Cu(II) couple in free form ($E_f{}^o$), which are taken as the average of E_{Pc} and E_{Pa}, are −0.89, −0.90 and −0.91 V for the complexes **1, 2** and **3**. On the addition of CT DNA with complexes, the voltammetric peak currents decreased apparently, indicating that there exist interactions between the complexes and CT DNA [51]. The drop of the voltammetric currents in the presence of CT DNA may be attributed to slow diffusion of the complexes (**1, 2** and **3**) bound to DNA. The cathodic (E_{Pc}) and anodic peak (E_{Pa}) potentials are found to be −1.01 and −0.72 V for the complex **1**, −1.06 and −0.75 V for the complex **2** and −0.99 and −0.67 V for the complex **3**. It can be seen that the peak-to-peak separation becomes larger, as ΔE_p = 0.29, 0.31 and 0.32 V for the complexes **1, 2** and **3** respectively, suggesting that in the presence of CT DNA the electron-transfer process becomes less reversible for the complexes. The formal potentials of the Cu(I)/ Cu(II) couple in binding form ($E_b{}^o$) are −0.86, -0.91 and −0.83 V for complexes **1, 2** and **3** respectively. Clearly, the values of the three complexes are shifted towards positive region by 0.03, 0.01 and 0.08 V for the complexes **1, 2** and **3** respectively, suggesting that the complexes could intercalate to DNA [52]. The separation between $E_b{}^o$ and $E_f{}^o$ can be used to estimate the ratio of binding constants for the reduced and oxidized forms to DNA using the equation as follows:

$$E_b - E_f = 0.059\ log\ [K_{CU(I)}\ /\ K_{CU(II)}]$$

Where $K_{Cu(I)}$ and $K_{Cu(II)}$ are the binding constant of Cu(I) and Cu(II) forms to DNA, respectively. The $K_{Cu(I)}/K_{Cu(II)}$ values were estimated to be 3.22, 1.46 and 3.32 for the complexes **1, 2** and **3** respectively. The shift in the anodic and cathodic peak potentials towards more positive side and the stronger affinity for less positively charged redox form indicating that the reduced forms of the complexes can interact more strongly than the oxidized ones. And this agreed with the intercalation mode of binding over electrostatic interaction mode. In the case of intercalation +1 form copper bound more strongly than +2 form of copper, probably because of the importance of hydrophobic interactions.

3.5. Protein binding studies

3.5.1. Absorbance and fluorescence studies

ACCEPTED MANUSCRIPT

UV-visible absorption measurement is a simple method to investigate the structural changes and to know which type of quenching occurs either dynamic or static quenching. The dynamic quenching refers to a process in which the fluorophore and the quencher come into contact during the transient existence of the excited state while static quenching refers to fluorophore–quencher complex formation in the ground state. The absorption band obtained for BSA at 278 nm in the absence of quencher when addition of the complexes (**1**, **2** and **3**) to BSA lead to an increase in BSA absorption intensity without affecting the position of absorption band. This indicates that the type of interaction between Cu(II) complexes and BSA was mainly a static quenching process [53]. The representative absorption titration spectra is shown in Fig. 13.

Fluorescence emission spectroscopy is usually employed to determine the interaction ability of metal complexes with human serum albumin, which is the most abundant protein in plasma. To understand the mechanism of interaction between the complexes (**1, 2** and **3**) and BSA, fluorescence quenching experiments have been carried out. Generally, the fluorescence property of protein is caused by three intrinsic characteristics of the protein, mainly due to the presence of tryptophan, tyrosine and phenylalanine residues [54]. Fig. 14 and S5 shows the fluorescence emission spectra of BSA after the addition of complexes (**1**, **2** and **3**). When increasing amount of complex solution was added to a fixed quantity of BSA, fluorescence intensity at 345 nm decreases upto 54.1, 69.2 and 81.8% for complexes respectively, with hypochromic shift of 16, 19 and 12 nm for complexes **1**, **2** and **3** respectively. The blue shift primarily arises due to the presence of the active site of the protein in a hydrophobic environment. It suggested that interaction is taking place between the compounds and BSA [55]. The fluorescence quenching is described by the Stern-Volmer relation [56,57] $F^o/F = 1 + K_q$ [Q] where F^o and F demonstrate the fluorescence intensities in the absence and presence of quencher, respectively. K_q is a linear Stern-volmer quenching constant, and [Q] is the quencher concentration. The quenching constant (K_q) can be calculated using the plot of log (F^o/F) *versus* log [Q] (Fig. 15). When small molecules bind independently to a set of equivalent site, on a macromolecule, the equilibrium between free and bound molecules is represented by the Scatchard equation. $\log[(F^o–F)/F] = \log K_b + n \log[Q]$ where K_b is the binding constant of the complex with BSA and n is the number of binding sites. From the plot of $\log[(F^o–F)/F]$ *versus* log[Q] (Fig.16), the number of binding sites (n) and the binding constant (K_b) values have been obtained. The quenching constant (K_q), binding constant (K_b) and number of binding sites (n) for

ACCEPTED MANUSCRIPT

the interaction of the Cu(II) complexes with BSA are shown in Table 7. In all the complexes, only one binding site is available to interact with BSA. Results showed that complexes **3** interact strongly with BSA compared to **2** and **1**.

3.5.2. Characteristics of synchronous fluorescence spectra

Synchronous fluorescence spectroscopy provides sound information about the molecular microenvironment, particularly in the vicinity of the fluorophore functional groups, the structural changes occurring to BSA upon the addition of the Cu(II) complexes. It is well-know that the fluorescence of BSA is normally, due to the presence of tyrosine, tryptophan and phenylalanine residues are responsible for the fluorescence property of BSA. According to miller, the difference between the excitation and emission wavelength ($\Delta\lambda = \lambda_{em} - \lambda_{exc}$) reflects the spectra of a different nature of chromophores, [58] with large $\Delta\lambda$ value, such as 60 nm, is characteristic of tryptophan residue and a small $\Delta\lambda$ value, such as 15 nm, is characteristic of tyrosine. The synchronous fluorescence spectra of BSA with various concentrations of Cu(II) complexes (**1, 2** and **3**) were recorded at $\Delta\lambda$ = 15 nm and $\Delta\lambda$ = 60 nm. On addition of the complexes, the fluorescence intensity of tryptophan residue at 340 nm decreased in the magnitude of 70.3, 73.8 and 83.3% for complexes **1**, **2** and **3** respectively (Fig. 17 and S6). Similarly, there was also decrease in the intensity of tyrosine residue at 300 nm. The magnitude of decrease was 43.3, 65.3 and 70.8% for complexes **1**, **2** and **3** respectively (Fig. 18 and S7). The synchronous fluorescence spectral studies clearly suggested that the fluorescence intensities of both the tryptophan and tyrosine were affected with increasing concentration of the complexes. The results indicate that the interaction of complexes with BSA affects the conformation of both tryptophan and tyrosine micro-region [59].

3.6. DNA cleavage

The cleaving efficacy of complexes (**1, 2** and **3**) has been assessed by their ability to convert supercoiled pUC19 DNA from form I to form II by agarose gel electrophoresis. As shown in (Fig. 19), no distinct DNA cleavage was observed for the control in which the complex was absent (lane 1); however, with fixed concentration of the complexes (**1, 2** and **3**), cleave SC (Form I) DNA into nicked circular (NC) (Form II) DNA, Hence, the complexes exhibited DNA cleavage activity in the absence of an external agent [60]. Additionally, the amount of helical unwinding induced by the complex bound to SC DNA provides evidence for the intercalation

ACCEPTED MANUSCRIPT

mode of interaction between the complexes and DNA. The DNA cleavage activity of the complexes (**1, 2** and **3**) can be estimated from the percentage of cleavage (C) (Table 8).

3.7. In *vitro* cytotoxic activity evaluation by MTT assays

The cytotoxicity of the monometallic and bimetallic complexes toward MCF7 (human breast cancer cells) and A549 (human lung cancer cells) cells has been examined by using MTT assay [61] and compared with cyclophosphamide [IC_{50} = 6.58 μM (MCF7) and 22.36 μM (A549)] under identical conditions. Figs. 20 and 21 show the cytotoxicity of the complexes (**1**-**3**) after 24 h incubation on MCF7 and A549 cancer cell lines, respectively. Complexes **2** and **3** exhibited moderate cytotoxicity with IC_{50} values of 88.59 and 82.56 μM against A549 respectively. The same complexes showed half inhibition concentration of 120.68 and 110.34 μM against MCF7 cell line respectively. Complex **1** showed only least activity. The enhanced activity of complex **3** compared to complexes **1** and **2** may be due to its bimetallic structure. The results of the cytotoxicity coincides well with the DNA and protein binding ability of the complexes. The IC_{50} values of all the complexes are listed in Table 9.

4. Conclusion

Two monometallic and one bimetallic copper(II) complexes with N-alkylated isatin based thiosemicarbazone ligands have been synthesized and characterized. Single crystal X-ray diffraction studies revealed that the **2** have square planar and **3** have square pyramidal geometry. The DNA binding affinity of the complexes were valuated using spectrophotometric methods. The results supported the interaction of the complexes with CT DNA through intercalation. Complexes **3** have better DNA cleaving ability compared to the other complexes. Fluorescence quenching experiments of BSA confirms the binding ability of the complexes and the mode of binding is static. In addition, the synchronous spectral investigations revealed that the complexes induced a small change in the secondary structure of the protein at the studied conditions. All complexes exhibited good cytotoxicity against cancer cell line A549and MCF7.

Electronic supplementary information (ESI) available: Crystallographic data for the structures reported in this paper have been deposited with the Cambridge Crystallographic Data Centre (CCDC) as supplementary publication numbers (CCDC 1418911, CCDC 1418910, CCDC 1418912, CCDC 1470836 and CCDC 1470837 for **L1, L2, L3, 2** and **3** respectively

ACCEPTED MANUSCRIPT

References

1 J. Anastassopoulou and T. Theophanides, in "Handbook *on Metal Ligand Interactions in Biological Fluids*", (ed. Guy Berton), **1994**, **p.1**, Vo 2. Part Five, Chap. 2.

2 P. Krishnamoorthy, P. Sathyadevi and T. Muthiah, *RSC Adv*., 2012, **2**, 12190–12203.

3 H. Dutler and AAmbar, In "*The Coordination Chemistry of Metalloenzymes* (eds., I. Bertini, S.R. Drago and C. Lucchinat) NATO Adv., Study lust. Series, Reidel: Dordrecht, 1991, 135.

4 B. Rosenberg, L.VanCamp, J. E. Troskov and V. H. Monsour, *Nature* (London) 1969, **222**, 385–386.

5 Kang Zheng, Liu Jiang, Yan-Tuan Li, Zhi-Yong Wu and Cui-Wei Yan *RSC Adv*., 2015, **5**, 51730–51744.

6 V. Rajendiran, M. Murali, E. Suresh, S. Sinha, K. Somasundaram and M. Palaniandavar, *Dalton Trans*., 2008, **6**, 148–163.

ACCEPTED MANUSCRIPT

7 B. Neto and A. Lapis, *Molecules*., 2009, **14**, 1725–1746.

8 C. Santini, M. Pellei, V. Gandin, M. Porchia, F. Tisato and C. Marzano, *Chem. Rev*., 2014, **114**, 815–862.

9 J. Yuan, D. B. Lovejoy, D. R. Richardson, *Blood*., 2004, **104**, 1450.

10 R. Ruiz, B. Garcia, J. Garcia-Tojal, N. Busto, S. Ibeas, J. M. Leal, C. Martins, J. Gaspar, J. Borras, R. Gil-Garcia, M. Gonzalez-Alvarez, *J. Biol. Inorg. Chem*., 2010, **15**, 515.

11 B. Lovejoy David, J. Jansson Patric, T. Brunk Ulf, J. Wong, P. Ponka, R. Richardson Des, *Cancer Res*., 2011, **71**, 5871–5880.

12. Duraippandi Palanimuthu, Sridevi Vijay Shinde, Kumaravel Somasundaram, and Ashoka G. Samuelson, *J. Med. Chem*., 2013, **56**, 722–734

13 F. Xue, C. Z. Xie, Y. W. Zhang, Z. Qiao, X. Qiao, J. Y. Xu and S. P. Yan, *J. Inorg. Biochem*., 2012, **115**, 78–86.

14 P. R. Chetana, R. Rao, D. Lahiri, R. S. Policegoudra, R. Sankolli and M. S. Aradhya, *Polyhedron*, 2014, **68**, 172–179.

15 Fang-Hong He, Lin Tao, Xiao-Wen Li, Yan-Tuan Li, Zhi-Yong Wu and Cui-Wei Yan *New J. Chem.,* 2012, **36**, 2078–2087.

16 D. Lu, X. Zhao, Y. Zhao, B. Zhang, B. Zhang, M. Geng and R. Liu, *Food Chem. Toxicol*., 2011, **49**, 3158–3164.

17 P. Bolel, N. Mahapatra, S. Datta and M. Halder, *J. Agric. Food Chem*., 2013, **61**, 4606–4613.

18 Sabeel M. Basheer, Anthony C. Willis, Ron J. Pace and Anandaram Sreekanth, *Polyhedron*, 2016, **109**, 7–18.

19 Jebiti Haribabu, Kumaramangalam Jeyalakshmi, Yuvaraj Arun, Nattamai S. P. Bhuvanesh, Paramasivan Thirumalai Perumalb and Ramasamy Karvembu, *RSC adv*., 2015, **5**, 46031–46049.

20 V. Philip, V. Suni, M. R. P. Kurup, M. Nethaji, *Polyhedron*, 2006, **26**, 1931-1938

21 F. A. French, E. J. Blanz Jr. *J. Med. Chem*., 1996, **9**, 585–589.

22 M. Das, S. E. Livingstone, *Br. J. Cancer*. 1978, **9**, 466–469.

23 A. S. Dobek, D. L. Klayman, E. T. Dickson, J. P. Scovill, E. C. Tramont, *Antimicrob. Agents Chemotherapy*. 1980, **18**, 27–36.

24 C. Shipman, J. R. Smith, J. C. Drach, D. L. Klayman, *Antiviral Res*., 1986, **6**, 197–222.

25 A. Usman, L. A Razak, S. Chantrapromma, H-K. Fun, A. Sreekanth, S. Sivakumar, M.R.P.

ACCEPTED MANUSCRIPT

Kurup, *Acta Cryst*, 2002, **8**, 461–463.

26 D. L. Klayman. A. J. Lin, J. W. McCall, *J. Med. Chem*., 1991, **38**, 1422–1425.

27 A. K. El-Sawaf, D. X. West, R. M. EI-Bahnasawy, F. A. EI-Saied, *Transition Met. Chem*, 1998, **23**, 227–232.

28 APEX2, Program for Data Collection on Area Detectors, BRUKER AXS Inc., 5465 East Cheryl Parkway, Madison, WI 53711–5373, USA.

29 Sheldrick, G.M. "*Program for Absorption Correction of Area Detector Frames*", BRUKER AXS Inc., 5465 East Cheryl Parkway, Madison, WI 53711-5373 USA

30 G. M. Sheldrick, Acta Crystallogr. Sect. A: Found. *Crystallogr*., 2008, **64**, 112–122.

31 O. V. Dolomanov, L. J. Bourhis, R. J. Gildea, J. A. K. Howard and H. Puschmann, *J. Appl. Crystallogr*., 2009, **42**, 339–341.

32 M. E. Reichmann, S. A. Rice and P. Thomas, *J. Am. Chem. Soc*., 1954, **76**, 3047–3053.

33 G. Cohen and H. Eisenberg, *Biopolymers*. 1969, **8**, 45.

34 T. J. Mossman, Immunol. *Methods*. 1983, **65**, 55.

35 J. P. Scovill, D. L. Klayman, C. F. Franchino, 2-Acetylpyridine thiosemicarbazones. 4. Complexes with transition metals as antimalarial and antileukemic agents. *J. Med. Chem*. 1982, **25**, 1261–1264.

36 Mathiyan Muralisankar, Nattamai S. P. Bhuvanesh and Anandaram Sreekanth *New J. Chem*., 2016, **40**, 2661–2679.

37 Mani Alagesan, Nattamai S.P. Bhuvanesh and Nallasamy Dharmaraj, *Dalton Trans*., 2014, **43**, 6087-6099

38 Anantharam Sreekanth, Maliyeckal R. Prathapachandra Kurup, *Polyhedron*, 2003, **20** 3321–3332.

39 S. Cunha, M. T. Rodrigues, C. C. de Silva, H. B. Napolitano, I. Vencato and C. Laricci, *Tetrahedron*, 2005, **61**, 10536-10540.

40 S. S. Batsanov, *J. Mol. Struct*., 2011, 990, 63-66.

41 B. Cordero, V. Gomez, A. E. Platero-Prats, M. Reves, J. Echeverria, E. Cremades, F. Barragan, S. Alvarez, *Dalton Trans*., 2008, 2832-2838.

42 A. Sreekanth, S. Sivakumar, M.R.P. Kurup, *J. Mol. Struct*. 2003, **655**, 47.

43 C.R. Comman, K.M. Geiser-Bush, S.P. Rowley, P.D. Boyle, *Inorg. Chem*. 1997, **36,** 6401.

ACCEPTED MANUSCRIPT

44 A. Sreekanth, V. Suni, Rohith P. John, Munirathinam Nethaji and M. R. Prathapachandra Kurup *Acta Cryst*. 2005, **61**, 284–286.

45 Kumaramangalam Jeyalakshmi, Nagamani Selvakumaran, Nattamai S.P. Bhuvanesh, Anandaram Sreekanth and Ramasamy Karvembu, *RSC Adv*., 2014, **4**, 17179-17195.

46 A. M. Pyle, J. P. Rehmann, R. Meshoyrer, C. V. Kumar, N. J. Turro and J. K. Barton, *J. Am. Chem. Soc*., 1989, **111**, 3051–3058.

47 A. Wolf, G. H. Shimer and T. Meehan, *Biochemistry*., 1987, **26**, 6392–6396.

48 Kumaramangalam Jeyalakshmi, Yuvaraj Arun, Nattamai SP Bhuvanesh, Paramasivan Thirumalai Perumal, Anandaram Sreekanth, Ramasamy Karvembu Inorganic Chemistry Frontiers 2015, **2**, 780–798.

49 Nagamani Selvakumaran, Nattamai S.P. Bhuvanesh and Ramasamy Karvembu, *Dalton Trans*., 2014, **43**, 16395–16410.

50 S. Mahadevan, M. Palaniandavar, Spectroscopic and voltammetric studies on copper complexes of 2,9-dimethyl-1,10-phenanthrolines bound to calf thymus DNA, *Inorg. Chem*., 1998, **37**, 693–700.

51 Y. M. Song, P. J. Yang, M. L. Yang, J. W. Kang, S. Q. Qin, B. Q. Lü, Spectroscopic and voltammetric studies of the cobalt(II) complex of morin bound to calf thymus DNA, *Transition Met. Chem*., 2003, **28**, 712–716.

52 M. T. Carter, M. Rodriguez, A. J. Bard, Voltammetric studies of the interaction of metal chelates with DNA. 2. Tris-chelated complexes of cobalt(III) and iron(II) with 1,10-phenanthroline and 2,2'-bipyridine, *J. Am. Chem. Soc*., 1989, **11**, 8901–8911.

53 D. Senthil Raja, G. Paramaguru, N. S. P. Bhuvanesh, J. H. Reibenspies, R. Renganathan and K. Natarajan, *Dalton Trans*., 2011, **40**, 4548–4559.

54 S. K. Leung, K. Y. Kwok, K. Y. Zhang, and K. K. Wing Lo, *Inorg. Chem*., 2010, **49**, 4984–4995.

55 D. Senthil Raja, N. S. P. Bhuvanesh and K. Natarajan, *Eur. J. Med. Chem*., 2011, **46**, 4584–4594.

56 J. R. Lakowicz, Fluorescence Quenching: Theory and Applications. *Principles of Fluorescence Spectroscopy*, Kluwer Academic/Plenum Publishers, New York 1999, 53–127.

57 X. Z. Feng, Z. Yang, L. J. Wang and C. Bai, *Talanta*., 1998, **47**, 1223–1229.

ACCEPTED MANUSCRIPT

58 G. W. Zhang, Q. M. Que, J. H. Pan and J. B. Guo, *J. Mol. Struct*., 2008, **881**, 132–138.

59 A. N. Glazer and E. L. Smith, *J. Biol. Chem*., 1961, **236**, 2942–2947.

60 Mathiyan Muralisankar, Jebiti Haribabu, Nattamai S.P. Bhuvanesh, Ramasamy Karvembu and Anandaram Sreekanth, Inorganica, Chimica, Acta., 2016, **449,** 82–95

61 P. Kumar, S. Gorai, M. Kumar Santra, B. Mondal and D. Manna, *Dalton Trans*., 2012, **41**, 7573–7581.

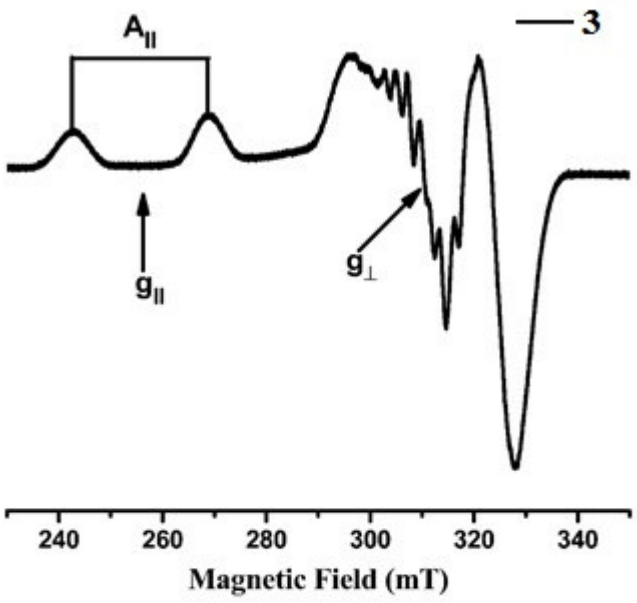

Fig. 1 EPR spectrum of complex **3** in frozen DMF solution. Microwave power, 0.98 mW; microwave frequency, 9.1 GHz.

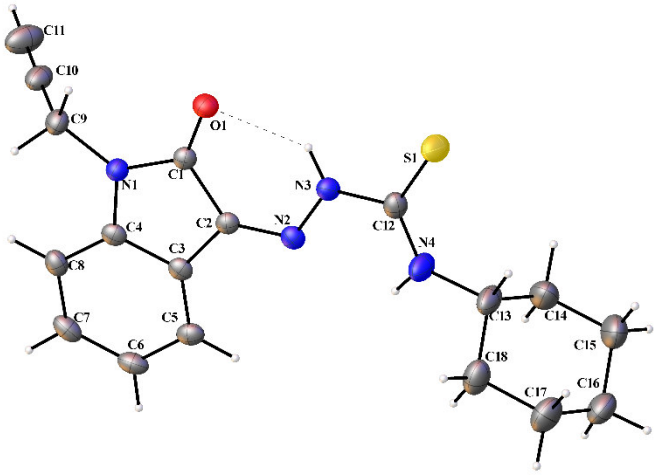

ACCEPTED MANUSCRIPT

Fig. 2 The molecular structure of ligand **L1**, with displacement ellipsoids drawn at the 50% probability level.

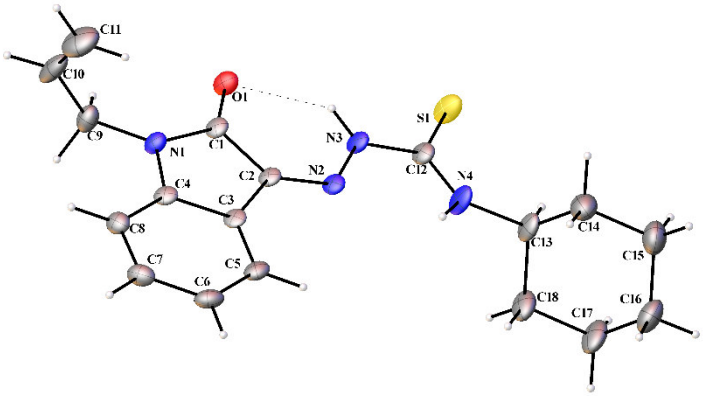

Fig. 3 The molecular structure of ligand **L2**, with displacement ellipsoids drawn at the 50% probability level.

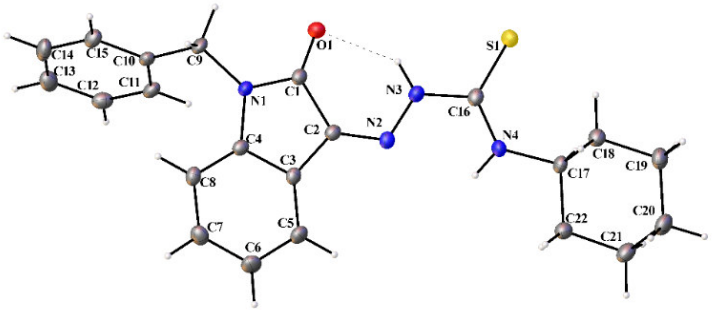

Fig. 4 The molecular structure of ligand **L3**, with displacement ellipsoids drawn at the 50% probability level.

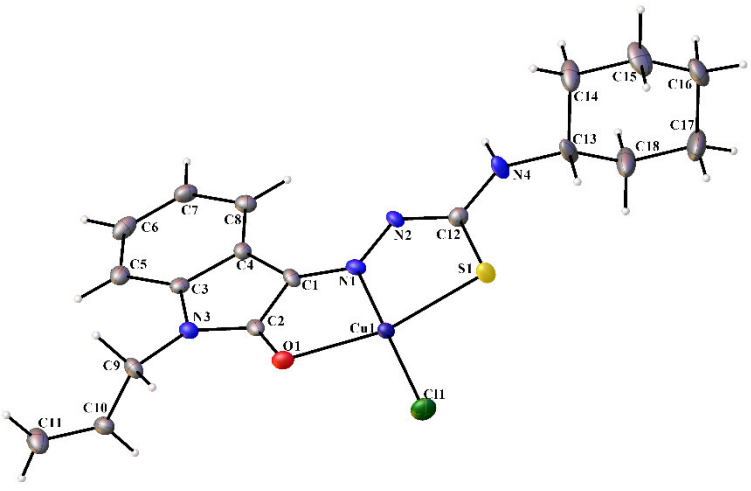

ACCEPTED MANUSCRIPT

Fig. 5 The molecular structure of complex **2**, with displacement ellipsoids drawn at the 50% probability level.

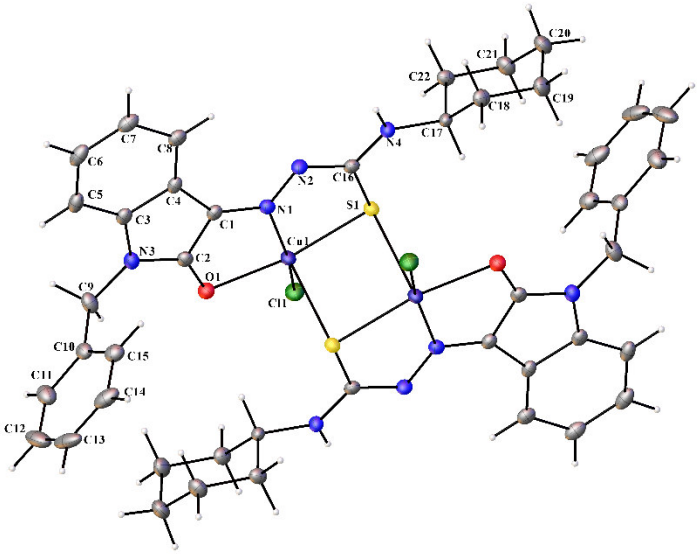

Fig. 6 The molecular structure of complex **3**, with displacement ellipsoids drawn at the 50% probability level.

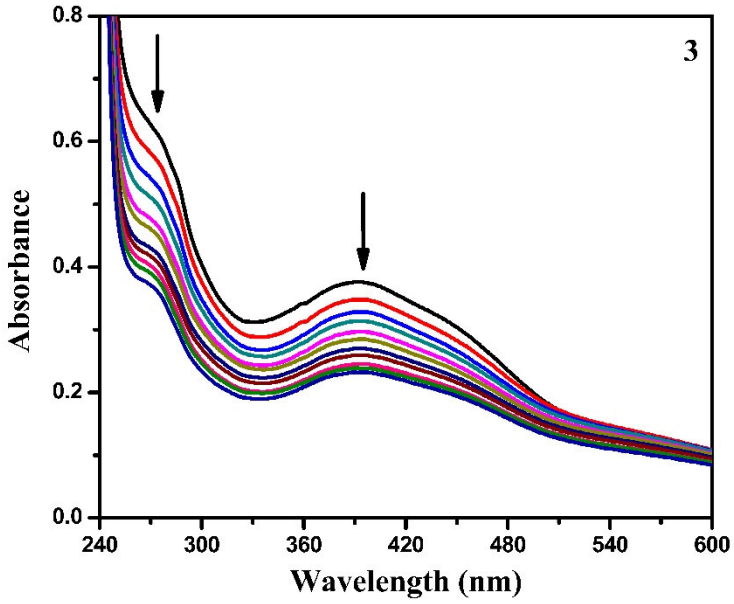

ACCEPTED MANUSCRIPT

Fig. 7 Absorption spectra of complex **3** in Tris-HCl buffer upon addition of CT DNA. [Complex] = 1.5 × 10^{-5} M, [DNA] = 0-50 μM. Arrow shows that the absorption intensities decrease upon increasing DNA concentration.

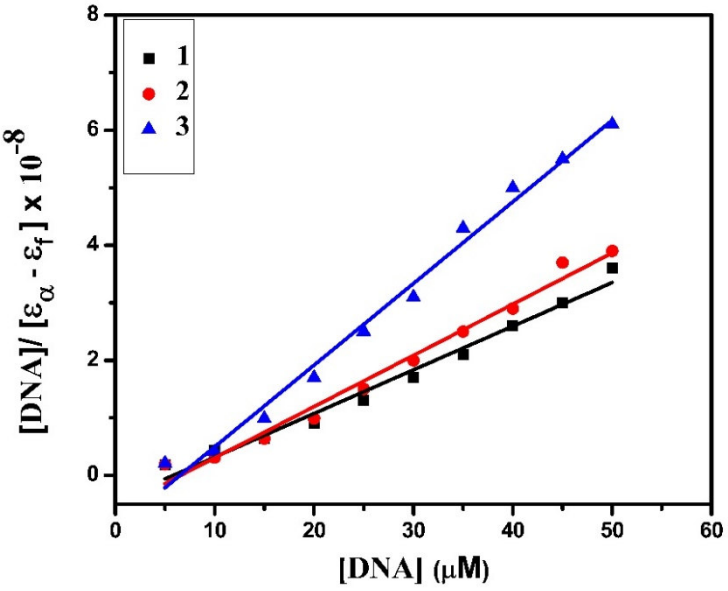

Fig. 8 Stern-Volmer plots of absorbance titrations of the complexes with CT DNA.

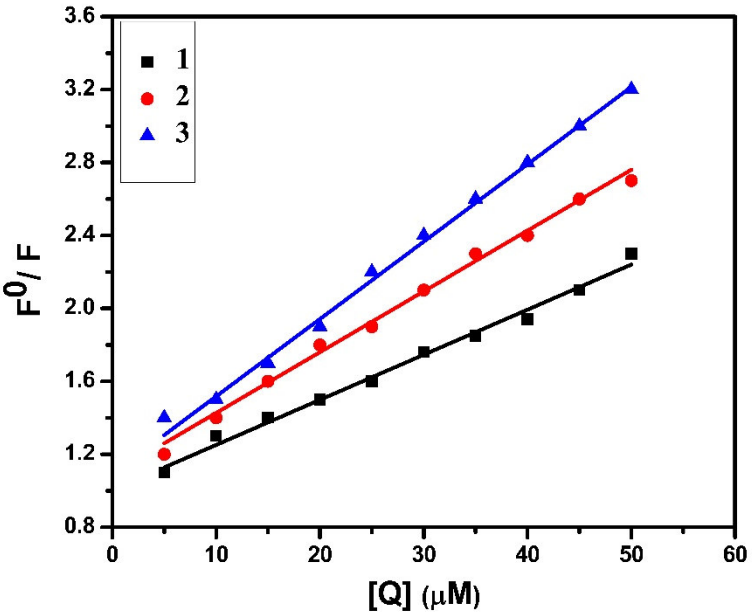

Fig. 9 Stern-Volmer plots of fluorescence titrations of the complexes with CT DNA.

ACCEPTED MANUSCRIPT

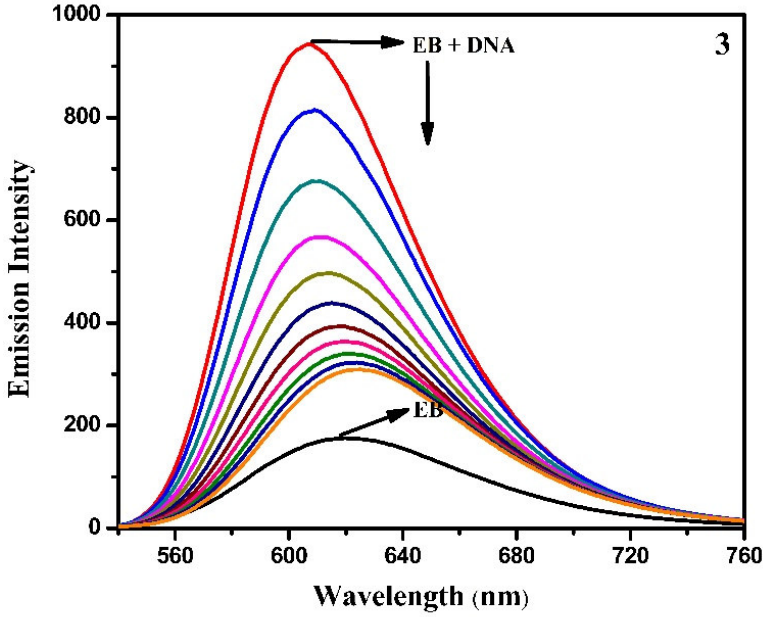

Fig. 10 Fluorescence quenching curves of EB bound to DNA in the presence of complex **3**. [DNA] = 5 µM, [EB] = 5 µM and [complex] = 0-50 µM.

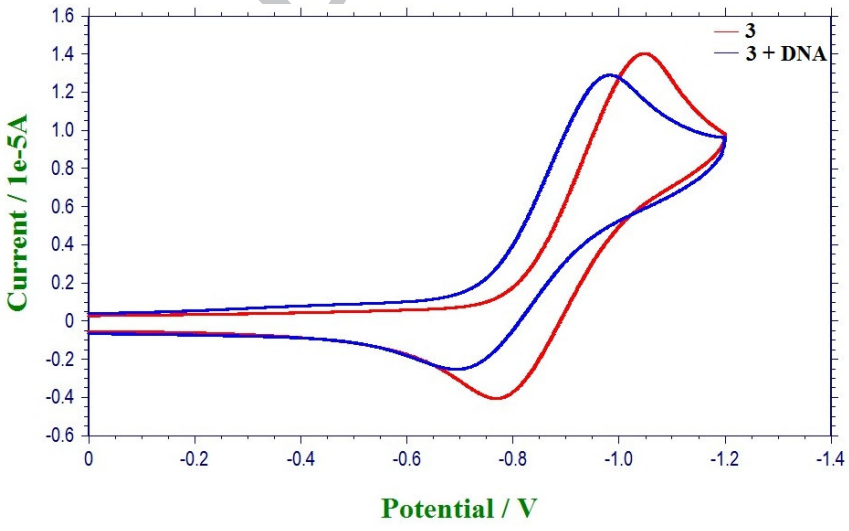

Fig. 11 Cyclic voltammograms of the complex (**3)** in the absence (red line) and presence (blue line) of CT-DNA.

ACCEPTED MANUSCRIPT

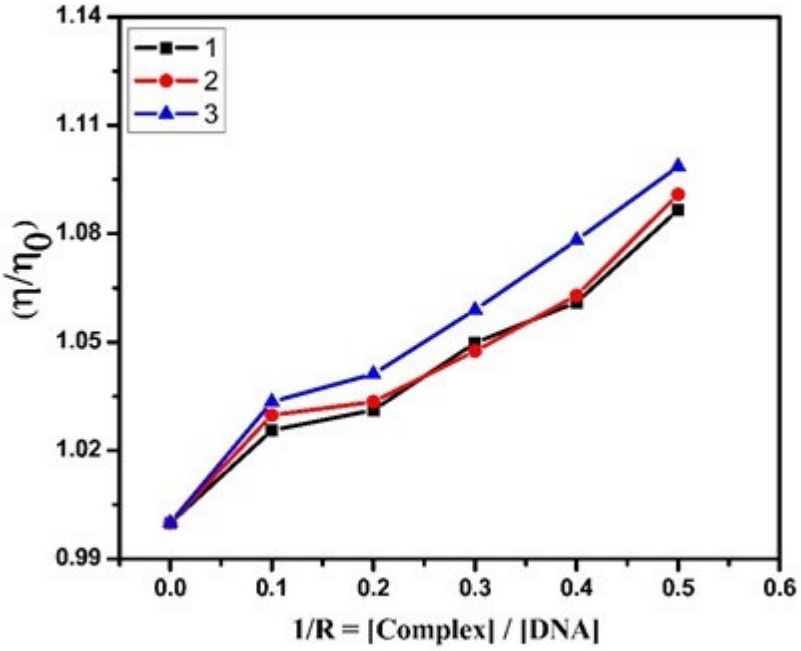

Fig. 12 Effect of the complexes on the viscosity of CT DNA (0.5 M).

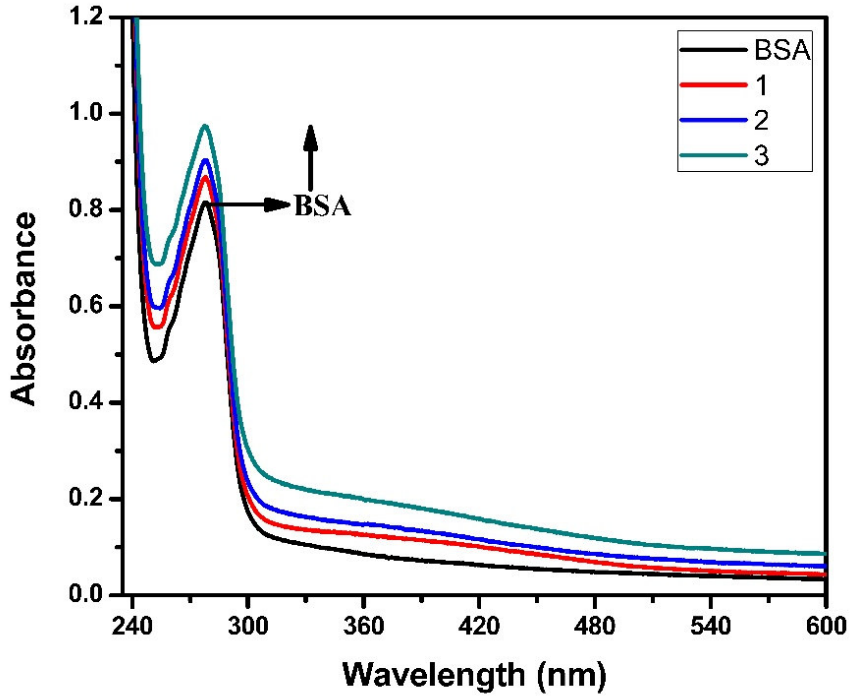

Fig. 13 The absorption spectra of BSA (10 μM) and BSA with (**1, 2** and **3)** (4 μM).

ACCEPTED MANUSCRIPT

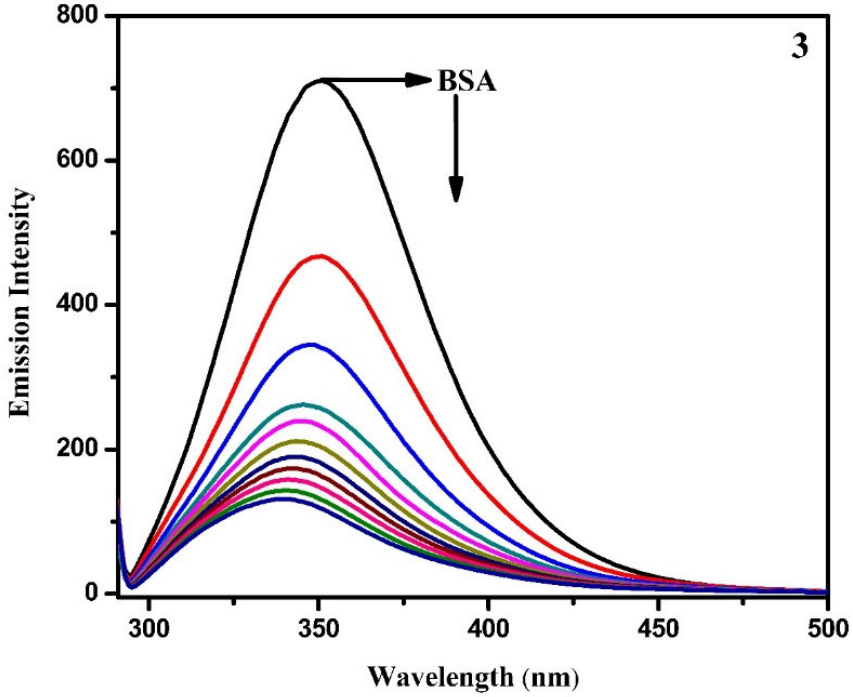

Fig.14 Fluorescence quenching curves of BSA in the absence and presence of complex **3** [BSA] = 1 μM and [complex] = 0-20 μM.

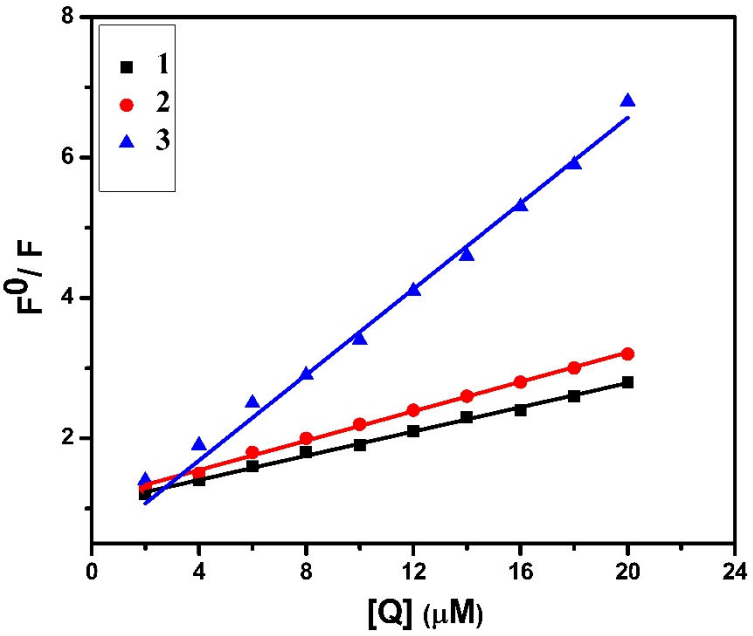

Fig. 15 Stern-Volmer plots of the fluorescence titrations of the complexes with BSA.

ACCEPTED MANUSCRIPT

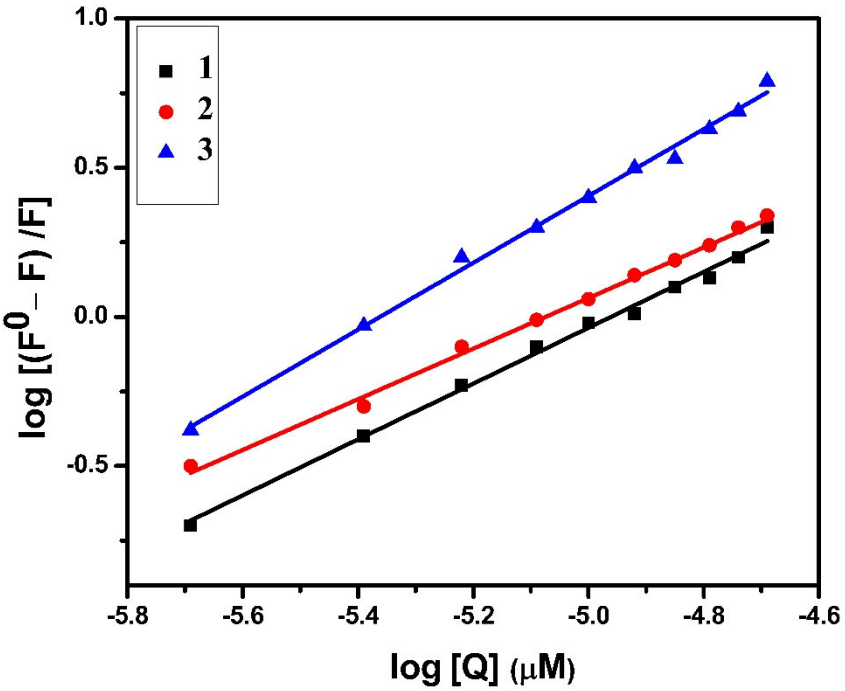

Fig. 16 Scatchard plots of the fluorescence titrations of the complexes with BSA.

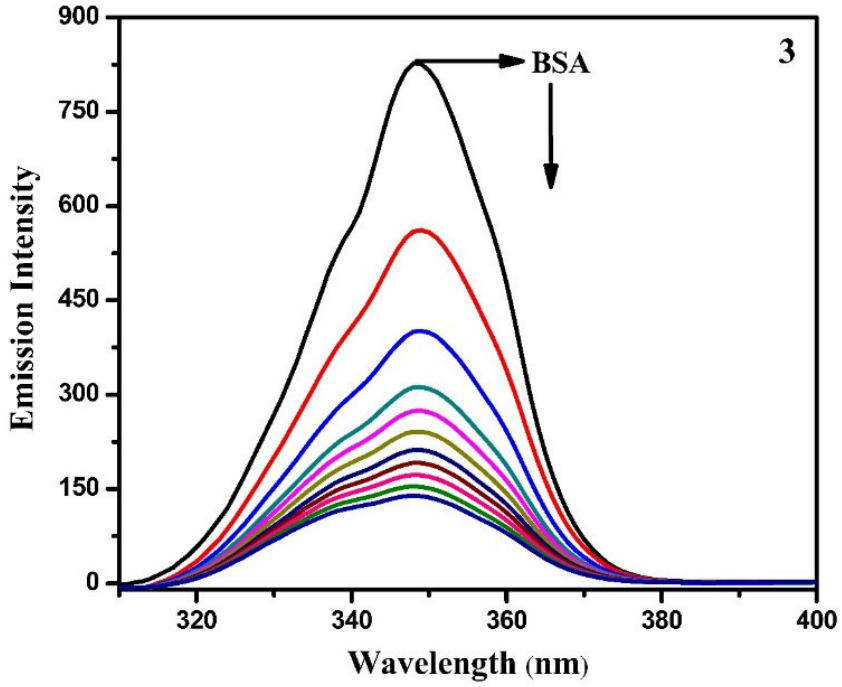

Fig. 17 Synchronous spectra of BSA (1 μM) as a function of concentration of complex **3** (0-20 μM) with $\Delta\lambda$ = 60 nm.

ACCEPTED MANUSCRIPT

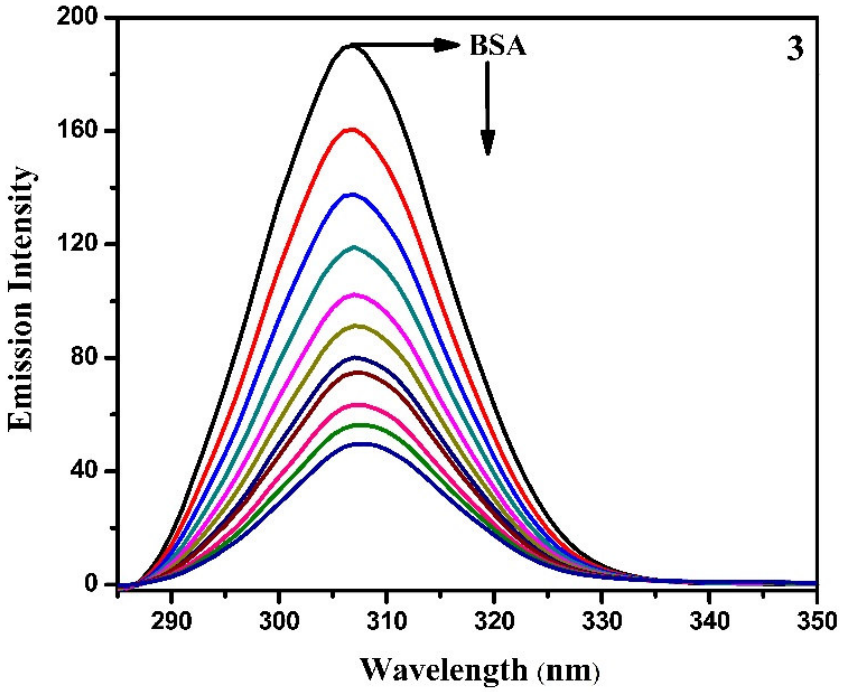

Fig. 18 Synchronous spectra of BSA (1 μM) as a function of concentration of complex 3 (0-20 μM) with $\Delta\lambda$ = 15 nm.

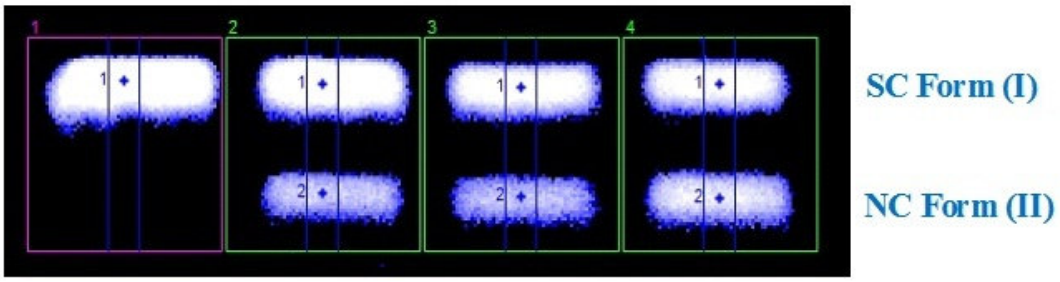

Fig. 19 Cleavage of supercoiled pUC19 DNA (30 μM) by complexes **1, 2** and **3** in a buffer containing 5% DMF/5 mM Tris–HCl/50 mM NaCl at pH = 7.2 and 37 ^{o}C with an incubation time of 3 h. lane 1, DNA control; lane 2, DNA + 1 (150 μM); lane 3, DNA + 2 (150 μM); lane 4, DNA + 3 (150 μM). Forms SC and NC are supercoiled and nicked circular DNA, respectively.

ACCEPTED MANUSCRIPT

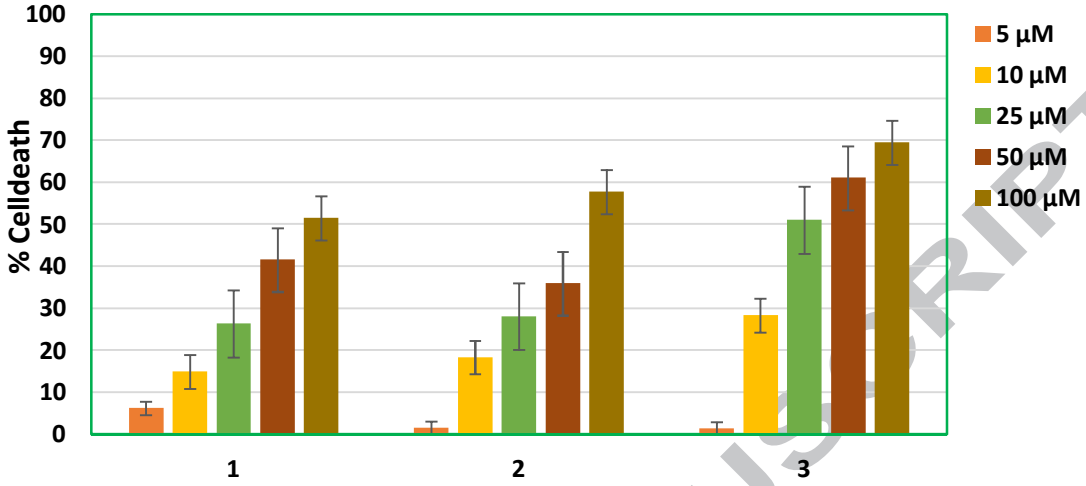

Fig. 20 Cytotoxicity of 1, 2 and 3 after 24 h incubation on A549 cell lines.

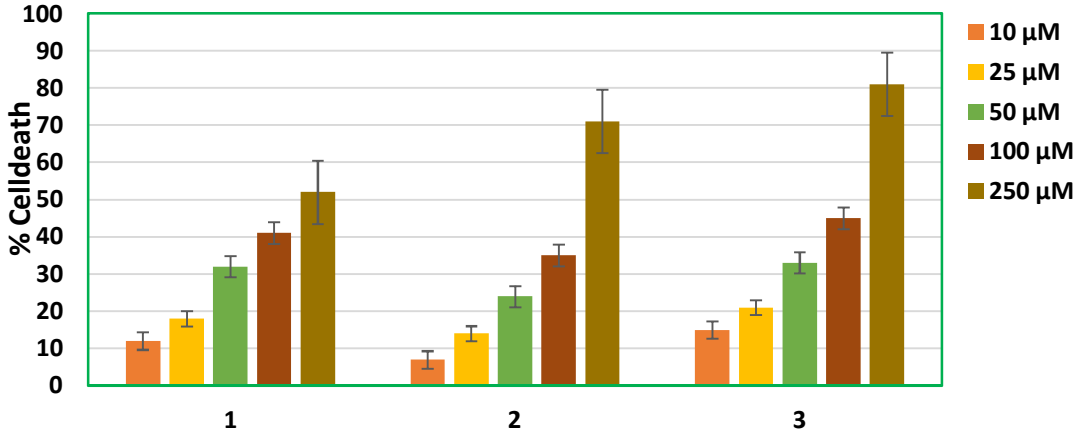

Fig. 21 Cytotoxicity of 1, 2 and 3 after 24 h incubation on MCF7 cell lines.

Table 1 EPR parameters of Cu(II) complexes

Complex	Medium & Temp.	$g_{\|}$	$g\perp$	$A_{\|}$ (MHz)
1	Solution state LNT	2.25	2.04	495
2	Solution state LNT	2.22	2.02	531
3	Solution state LNT	2.24	2.05	524

ACCEPTED MANUSCRIPT

Table 2 Crystal data and structure refinement for L1, L2 and L3

	L1	**L2**	**L3**
Empirical formula	$C_{18}H_{20}N_4OS$	$C_{18}H_{22}N_4OS$	$C_{22}H_{24}N_4OS$
Formula weight	340.44	342.45	392.51
Temperature (K)	150.15	150.15	110.15
Wavelength (Å)	0.71073	0.71073	0.71073
Crystal system	Triclinic	Monoclinic	Triclinic
Space group	*P* - 1	*P* 1 2_1/c 1	*P* - 1
Unit cell dimensions			
a (Å)	6.517(4)	6.567(2)	9.040(3)
b (Å)	8.453(5)	8.352(3)	10.738(3)
c (Å)	16.366(9)	32.372(10)	11.191(3)
α(°)	95.674(5)	90	93.781(3)
β(°)	90.280(6)	91.899(4)	111.505(3)
γ(°)	98.757(6)	90	97.842(3)
Volume (Å^3)	886.5(8)	1774.5(9)	993.2(5)
Z	2	4	2
Density Mg/m^3	1.275	1.282	1.312
Absorption coefficient (mm^{-1})	0.195	0.195	0.183
F(000)	360	728	416
Crystal size (mm^3)	0.45 x 0.38 x 0.19	0.54 x 0.54 x 0.22	0.52 x 0.47 x 0.19
Theta range for data collection (°)	2.450 to 27.604	2.518 to 27.595	1.930 to 27.508
Index ranges	-8<=h<=8, -10<=k<=10, -21<=l<=20	-8<=h<=8, -10<=k<=10, -41<=l<=41	-11<=h<=11, -13<=k<=13, -14<=l<=14
Reflections collected	10283	30846	11676
Independent reflections [R(int)]	4001 (0.0288)	4076 (0.0645)	4507 (0.0274)
Completeness to theta = 27.50°	99.8 %	99.8 %	99.6 %
Absorption correction	Semi-empirical from equivalents	Semi-empirical from equivalents	Semi- empirical from equivalents
Max. and min. transmission	0.7456 and 0.6717	0.7456 and 0.3564	0.7456 and 0.6619
Refinement method	Full-matrix least-squares on F^2	Full-matrix least-squares on F^2	Full-matrix least-squares on F^2

ACCEPTED MANUSCRIPT

Data / restraints / parameters	4001 / 0 / 217	4074 / 0 / 217	4507 / 0 / 253
Goodness-of-fit on F^2	1.040	1.097	1.024
Final R indices [I>2sigma(*I*)]	R1 = 0.0391, wR2 = 0.0947	R1 = 0.0494, wR2 = 0.1199	R1 = 0.0373, wR2 = 0.0929
R indices (all data)	R1 = 0.0477, wR2 = 0.1001	R1 = 0.0547, wR2 = 0.1232	R1 = 0.0435, wR2 = 0.0970
Largest diff. peak and hole (e.Å^{-3})	0.311 and -0.263	0.598 and -0.369	0.343and -0.308

Table 3 Crystal data and structure refinement for 2 and 3

	2	**3**
Empirical formula	C_{18} H_{21} Cl Cu N_4 O S	C_{44} H_{46} C_{12} Cu_2 N_8 O_2 S_2
Formula weight	440.44	980.99
Temperature (K)	99.99	100.0
Wavelength (Å)	0.17073	0.71073
Crystal system	Monoclinic	Monoclinic
Space group	*P - 1*	*P* 1 2_1/n 1
Unit cell dimensions		
a (Å)	6.6683(7)	8.5904(5)
b (Å)	8.9469(9)	23.9925(13)
c (Å)	16.0679(16)	10.9563(5)
α(°)	90.855(2)	90
β(°)	90.461(2)	109.355
γ(°)	97.099(2)	90
Volume (Å^3)	951.12(17)	2130.5(2)
Z	2	2
Density Mg/m^3	1.538	1.529
Absorption coefficient (mm^{-1})	1.413	1.271
F(000)	454	1012
Crystal size (mm^3)	0.408 x 0.19 x 0.066	0.353 x 0.205 x 0.032
Theta range for data collection (°)	2.536 to 27.593	2.601 to 27.523
Index ranges	-8<=h<=8, -11<=k<=11, 0<=l<=20	-11<=h<=11, -31<=k<=31, -14<=l<=14
Reflections collected	9328	84731
Independent reflections [R(int)]	9328	4890 (0.0339)

ACCEPTED MANUSCRIPT

ACCEPTED MANUSCRIPT

Completeness to theta = 27.50°	98.9 %	99.8 %
Absorption correction	Semi-empirical from equivalents	Semi- empirical from equivalents
Max. and min. transmission	0.746 and 0.552	0.7456 and 0.6512
Refinement method	Full-matrix least-squares on F^2	Full-matrix least-squares on F^2
Data / restraints / parameters	9328 / 0 / 236	4890 / 0 / 271
Goodness-of-fit on F^2	1.136	1.057
Final R indices [I>2sigma(*I*)]	R1 = 0.0511, wR2 = 0.1162	R1 = 0.030, wR2 = 0.0704
R indices (all data)	R1 = 0.0574, wR2 = 0.1185	R1 = 0.0343, wR2 = 0.0723
Largest diff. peak and hole (e.Å^{-3})	0.818 and -0.680	0.846 and -0.524

Table 4 Selected bond lengths (Å) and bound angles (°)

	L1	**L2**	**L3**
S(1)-C(12)	1.6723(16)	1.6696(18)	1.6723(14)
O(1)-C(1)	1.2253(16)	1.224(2)	1.2294(16)
N(1)-C(1)	1.3721(18)	1.380(2)	1.3708(16)
N(1)-C(9)	1.4528(18)	1.451(2)	1.4544(16)
N(2)-N(3)	1.3488(16)	1.3475(19)	1.3524(15)
N(3)-C(12)/C(12)/C(16)	1.3755(18)	1.379(2)	1.3813(17)
N(4)-C(12)/C(12)/C(16)	1.326(2)	1.326(2)	1.3355(17)
N(4)-C(13)/C(12)/C(17)	1.4569(19)	1.464(2)	1.4688(16)
N(4)-H(4)	0.8800	0.8800	0.8800
C(1)-C(2)	1.5001(19)	1.5002(2)	1.5055(17)
N(1)-C(1)-C(2)	105.69(11)	106.02(13)	105.93(10)
N(2)-N(3)-C(12)/C(12)/C(16)	119.30(12)	119.27(14)	120.16(11)
N(2)-N(3)-H(3)	120.4	120.4	119.9
N(3)-C(12)-S(1)	118.68(11)	118.79(13)	118.02(10)
N(4)-C(12)-S(1)	126.71(11)	126.63(13)	127.47(10)
N(4)-C(12)-N(3)	114.60(13)	114.58(15)	114.50(11)
O(1)-C(1)-N(1)	126.83(12)	126.71(15)	126.77(12)
O(1)-C(1)-C(2)	127.49(12)	127.27(15)	127.30(12)

ACCEPTED MANUSCRIPT

Table 5 Selected bond lengths (Å) and bound angles (°) 1[a]

2		**3**	
Cu(1)-Cl(1)	2.1920(10)	Cu(1)-Cl(1)	2.2140(5)
Cu(1)-S(1)	2.2362(11)	Cu(1)-S(1)#1	2.7763(5)
Cu(1)-O(1)	2.072(3)	Cu(1)-S(1)	2.2821(5)
Cu(1)-N(1)	1.970(3)	Cu(1)-O(1)	2.1069(13)
S(1)-C(12)	1.731(4)	Cu(1)-N(1)	1.9812(16)
O(1)-C(2)	1.252(5)	S(1)-Cu(1)#1	2.7763(5)
N(1)-N(2)	1.329(4)	S(1)-C(16)	1.7470(18)
N(2)-C(12)	1.353(5)	O(1)-C(2)	1.250(2)
N(3)-C(9)	1.464(5)	N(3)-C(9)	1.449(2)
N(4)-C(12)	1.325(5)	N(4)-C(16)	1.317(2)
N(4)-C(13)	1.463(5)	N(4)-C(17)	1.465(2)
Cl(1)-Cu(1)-S(1)	96.46(4)	Cl(1)-Cu(1)-S(1)	99.331(19)
O(1)-Cu(1)-Cl(1)	96.94(8)	Cl(1)-Cu(1)-S(1)#1	103.281(18)
O(1)-Cu(1)-S(1)	165.34(8)	O(1)-Cu(1)-Cl(1)	94.35(4)
N(1)-Cu(1)-Cl(1)	173.37(11)	O(1)-Cu(1)-S(1)	165.64(4)
N(1)-Cu(1)-S(1)	83.46(10)	O(1)-Cu(1)-S(1) #1	89.35(4)
N(1)-Cu(1)-O(1)	83.93(12)	N(1)-Cu(1)-Cl(1)	159.34(5)
N(2)-N(1)-Cu(1)	125.4(3)	N(1)-Cu(1)-S(1)	82.74(5)
N(2)-C(12)-S(1)	124.5(3)	N(1)-Cu(1)-O(1)	82.92(6)
N(4)-C(12)-S(1)	120.1(3)	N(2)-N(1)-Cu(1)	126.74(16)
N(4)-C(13)-C(14)	109.9(4)	N(2)-C(16)-S(1)	124.21(14)
C(12)-S(1)-Cu(1)	95.98(14)	N(4)-C(16)-S(1)	120.58(14)
C(2)-O(1)-Cu(1)	105.1(2)	C(16)-S(1)-Cu(1)	95.39(6)

[a] Symmetry transformations used to generate equivalent atoms: #1 -x+1,-y+1,-z+1

ACCEPTED MANUSCRIPT

ACCEPTED MANUSCRIPT

Table 6 DNA binding constant (K_b), Stern-Volmer constant (K_q) and the apparent binding constant (K_{app}) for complexes (**1, 2** and **3)**.

Complex	K_b (M^{-1})	K_q (M^{-1})	K_{app} (M^{-1})
1	1.49×10^5	2.47×10^4	1.24×10^6
2	1.52×10^5	3.33×10^4	1.66×10^6
3	1.72×10^5	4.24×10^4	2.12×10^6

Table 7 Protein binding constant (K_b), quenching constant (K_q) and number of binding sites (n) for complexes (**1, 2** and **3)**.

Complex	K_b (M^{-1})	K_q (M^{-1})	n
1	8.64×10^4	2.04×10^4	0.94
2	1.05×10^5	4.43×10^4	0.85
3	3.05×10^5	1.03×10^6	1.12

Table 8 Self-activated cleavage data of SC pUC19 DNA (30 μM) by complexes **1, 2** and **3** (150 μM) for an incubation time of 3 h.

Lane No	DNA control	Percentage of cleavage (C) (%)	
		SC (1)	NC (2)
1	DNA	100	0
2	DNA + **1** (150 μM)	65.16	35.89
3	DNA + **2** (150 μM)	63.12	36.88
4	DNA + **3** (150 μM)	54.57	45.43

Table 9 *In vitro* cytotoxic studies of Cu(II) complexes against MCF7 and A549 cancer cell lines

Complexes	IC 50	
	A549 (μM)	MCF7 (μM)
1	99.53	247.21
2	88.59	120.68
3	82.56	110.34
Cyclophosphamide	6.58	22.36

ACCEPTED MANUSCRIPT

Synthesis and crystal structure of new monometallic and bimetallic copper(II) complexes with N-substituted isatin thiosemicarbazone ligands: Effects of the complexes on DNA/protein-binding property, DNA Cleavage and cytotoxicity studies

Graphical abstract

New monometallic and bimetallic copper(II) complexes with N-substituted isatin thiosemicarbazone ligands have been synthesized and evaluated for its biological applications like DNA/protein binding, DNA cleavage and cytotoxicity studies.